Journal of Materials Chemistry A

ROYAL SOCIETY OF CHEMISTRY

REVIEW

View Article Online
View Journal | View Issue

Cite this: J. Mater. Chem. A, 2024, 12, 9296

Flexible resistive tactile pressure sensors

Qianhe Shu,[a] Yuncong Pang,[b] Qiqi Li,[a] Yuzhe Gu,[a] Zhiwei Liu, *[c] Baoguang Liu,[a] Jianmin Li*[a] and Yang Li *[ab]

Received 13th November 2023
Accepted 11th March 2024

DOI: 10.1039/d3ta06976a

rsc.li/materials-a

The widespread integration of sensors into our everyday existence has paved the path for groundbreaking progress across various domains, including healthcare, robotics, and human–computer interaction. In this context, flexible resistive tactile pressure sensors have emerged as vital instruments due to their outstanding electrical and mechanical properties, cost-effectiveness, and ease of manufacturing. They have become pivotal in driving innovation, from wearable devices to human–machine interfaces. This comprehensive review article delves into recent advancements in this rapidly growing field, focusing on operational principles, performance metrics, material choices, structural design, and the applications of flexible resistive tactile pressure sensors. The challenges and opportunities in the field, such as enhancing sensitivity, durability, and reproducibility, and emerging trends, such as the integration of machine learning algorithms for real-time data analysis are also addressed, providing insights into the future direction of this rapidly evolving technology. By consolidating the current state-of-the-art in flexible resistive tactile pressure sensors, this article aims to inspire further innovation and collaboration in the pursuit of more sophisticated and versatile tactile pressure sensing technologies.

1. Introduction

Sensors, serving as tools for collecting, detecting, converting, and transmitting information, possess the capability to convert target signals that are not directly measurable into electrical or other output signals following specific patterns.[1–5] The need for precise and versatile tactile pressure sensing is evident in numerous applications, spanning from the delicate touch needed in medical diagnostics to the responsive interaction vital in modern robotics. Serving as essential components in smart devices to comprehend the external surroundings, tactile sensors are primarily responsible for empowering devices to identify and perceive various physical attributes during the device's functioning while engaging with target objects and the surrounding milieu.[6–8] Nonetheless, traditional tactile sensors predominantly employ a variety of rigid materials as their sensitive components. Due to the substantial advancements in rigid electronic components and materials over time, sensor systems of various types have become inherently inflexible, leading to a standardization of their operational principles and environmental adaptability. In previous sensor applications, the key requirements were stability, cost-effectiveness, and durability, which rigid sensors could effectively address and fulfill for the majority of cases. However, as robotics continues to advance and the demand for high processing performance in sensors persists, sensors based on rigid materials have begun to exhibit numerous issues.[9] Despite their technological maturity, the constraints of form and material inherent to these sensors result in drawbacks such as bulkiness and fragility, which hinder their applicability in flexible human–machine interaction and portable wearable smart devices.

In contrast to "rigidity," flexibility in tactile sensors refers to human skin-like properties, including adaptability to diverse shapes, which ensures effective functionality across various technological domains.[10] Flexible sensors, which enhance surface contact for increased sensitivity, play a crucial role in applications like robotics, where precise pressure measurements are vital for safe and efficient interactions.[11] Furthermore, the relationship between flexibility and durability empowers sensors to withstand mechanical stress, proving advantageous in applications involving repetitive strains.[12]

In practical tactile perception, the forces acting on the sensor are highly complex, leading to intricate mechanical stimuli. Tactile sensors need to precisely perceive forces of various magnitudes and directions, generating electrical signals in real-time based on different operating principles to be transmitted to the system for analysis. Based on different ways of generating electrical signals, flexible tactile sensors can be classified into resistive,[13] capacitive,[14] inductive,[15] piezoelectric,[16] and triboelectric types.[17] Among them, researchers have focused extensively on flexible resistive tactile sensors due to their notable

[a]College of Electronic and Optical Engineering, College of Flexible Electronics (Future Technology), Nanjing University of Posts & Telecommunications (NJUPT), Nanjing, 210023, China. E-mail: lijm@njupt.edu.cn; yli@njupt.edu.cn

[b]State Key Laboratory of Organic Electronics and Information Displays, Jiangsu Key Laboratory for Biosensors, Institute of Advanced Materials (IAM), Nanjing University of Posts and Telecommunications (NJUPT), Nanjing, 210023, China

[c]School of Energy and Environmental Engineering, University of Science and Technology Beijing, Beijing 100083, China. E-mail: liuzhiwei@ustb.edu.cn

advantages, including high precision, sensitivity, a broad sensing range, uncomplicated structure, stability, reliability, ease of miniaturization, and robust overload capacity. In 2013, Canavese *et al.* proposed a piezoflexible resistive composite material that can be used to make flexible tactile sensors that achieve real-time 3D response to pressure and can be used for tactile sensing in robotics.[18] As more experiments were conducted, flexible tactile piezoresistive sensors were found to have good integration with humans in addition to robots. In 2015, flexible tactile sensors were made into electronic skin by Gerratt *et al.* and applied to the surface of human skin.[19] In pursuit of better portability and usage experience, after material optimization and structure design, Gao *et al.* developed a wearable microfluidic diaphragm pressure sensor in 2017.[20] This sensor is thinner, lighter, more sensitive, and has more comprehensive and detailed haptic feedback. In 2019, Wu built on this foundation by iterating on a sensor that can be self-powered.[21] Two years later, Wang *et al.* designed a self-powered tactile sensor with an even lower limit of pressure detection, opening up the possibility of ultra-small signal detection.[22] In 2022 and 2023, researchers' dedicated efforts and the integration of flexible tactile piezoresistive sensors into human–machine interaction, coupled with machine learning and material and structural optimization, significantly enhanced sensor performance, reaching an unprecedented level of sensitivity and practicality.[23,24]

Presently, there have been noteworthy and substantial advancements in the field of flexible resistive tactile sensors. The progression extends from the initial resistive rigid tactile sensors to the inception and evolution of the flexible tactile sensing concept. In aspects related to substrate materials, sensitive material choices, unit structures, and the design of integrated arrays, the manufacturing technology for flexible resistive tactile sensors has progressively matured, allowing for a wider range of functionalities (Fig. 1). In addition to detecting pressure and tension, numerous flexible resistive tactile sensors can also detect friction, torsion, bending force, temperature, humidity, proximity, and other physical stimuli. Some even

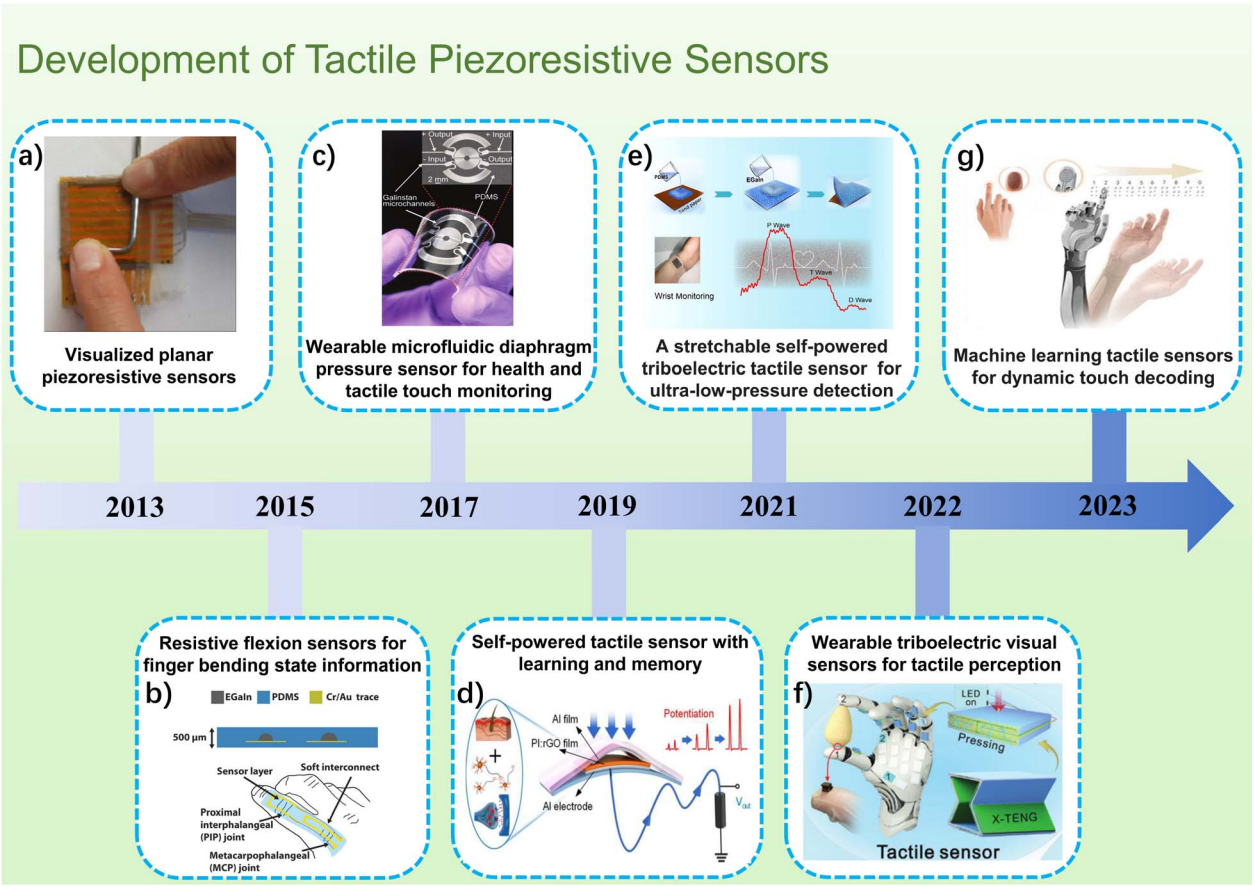

Fig. 1 The development of piezoresistive tactile sensors in recent years. (a) Polymeric composite with nanostructured spiky particles as filler.[18] Reproduced with permission. Copyright at *Sensors and Actuators A: Physical*, 2014 (b) schematic of the cross-section and graphical representation on a finger of the resistive flexion sensors for finger bending state information.[19] Reproduced with permission. Copyright at *Advanced Functional Materials*, 2015 (c) Wearable Microfluidic Diaphragm Pressure Sensor for Health and Tactile Touch Monitoring.[20] Reproduced with permission. Copyright at *Advanced Materials*, 2017 (d) Self-Powered Tactile Sensor with Learning and Memory.[21] Reproduced with permission. Copyright at *ACS Nano*, 2019 (e) A stretchable self-powered triboelectric tactile sensor with EGaIn alloy electrode for ultra-low-pressure detection.[22] Reproduced with permission. Copyright at *Nano Energy*, 2021 (f) Wearable Triboelectric Visual Sensors for Tactile Perception.[23] Reproduced with permission. Copyright at *Advanced Materials*, 2022 (g) Machine Learning-Enabled Tactile Sensor Design for Dynamic Touch Decoding.[24] Reproduced with permission. Copyright at *Advance Science*, 2023.

possess features such as transparency,[25] magnetism sensitivity,[26] and self-healing.[27] The refinement of performance and diversification of functionality have led them from perceiving force on objects to monitoring posture movements,[28] facial expressions,[29] physiological health,[30] and further into establishing tactile sensing systems, protecting against external environmental interference, and assisting in medical health monitoring.

In recent years, there has been a swift evolution in flexible resistive tactile sensors, characterized by the continuous emergence of new materials and structures, often accompanied by the development of high-performance sensors. To consolidate and synthesize this wealth of information, this review initiates with an exploration of the two fundamental detection principles underpinning flexible resistive tactile sensors. Additionally, it serves as a reference for researchers aiming to create novel materials and structures. Furthermore, the sensors' performance can be summarized using six key performance parameters based on empirical data. Subsequently, in the subsection of flexible substrates and conductive materials that most researchers are committed to innovating and optimizing, the vast variety of materials and common structural designs used in flexible resistive tactile sensors up to the present time are described in detail, and different types of flexible resistive tactile sensors are compared and analyzed. Finally, the three main application areas of the sensor are summarized: tactile sensing and human–computer interaction, healthcare, and electronic skin. While pointing out the advantages of flexible resistive tactile sensors, this subsection also identifies the technical challenges faced by current research and provides an outlook on their future development.

2. Principle of flexible resistive tactile sensors

In tactile sensing, pressure, strain and friction may exist. According to different tactile sensing methods, tactile sensors are classified into various types, including resistive, piezoelectric, capacitive, and friction-based. However, in practical applications, the signal output is actually multiple effects from mechanical stimuli. In order to enhance the signal output quality of tactile sensors, the combination of multiple sensing mechanisms has become an innovative improvement approach.[31–33] Among the various tactile sensors, resistive tactile sensors have garnered significant attention from scholars due to their relatively low cost, ease of manufacturing, and large sensitivity range, making them suitable for larger contact areas. Here, we provide a detailed description and explanation of the sensing principles of flexible resistive tactile pressure sensors. The unique qualities of flexible resistive tactile sensors are a direct result of their distinct sensing mechanism and operational concepts. By capitalizing on these two principles, researchers are committed to improving essential performance metrics that serve as critical indicators of overall functionality. This next section will provide a detailed exploration of the underlying rationale for optimizing materials and structures, offering insights into the two sensing principles and the six primary performance parameters of flexible resistive tactile sensors.

2.1. Detection principle of flexible resistive tactile sensors

In the realm of detection principles, flexible resistive tactile sensors can be broadly classified into two mechanisms: pressure-sensitive and resistive strain-sensitive mechanisms. While both mechanisms involve generating resistance responses to external stimuli and quantifying input signal magnitudes by monitoring variations in resistance values, it's important to note that their underlying principles differ.

2.1.1. Pressure-sensitive. Pressure-sensitive flexible resistive sensors are firstly created using the piezoresistive effect of single-crystal silicon material.[34] The piezoresistive effect refers to the phenomenon where the lattice of a silicon crystal deforms when force is applied, causing charge carriers to scatter from one energy valley to another, which changes the carrier mobility, perturbing the average quantity of carriers both longitudinally and transversely, leading to the changes of silicon's resistivity (Fig. 2a).[35] This variation varies with the crystal's orientation, making silicon's piezoresistive effect orientation-dependent.

Unlike traditional pressure-sensitive sensors, pressure-sensitive flexible resistive sensors use single-crystal silicon as the sensitive material, but they utilize substrates that are more flexible to enhance their deformation capabilities. When the single-crystal silicon material in a pressure-sensitive flexible resistive sensor experiences force, its resistivity undergoes a corresponding change.

2.1.2. Resistive strain-sensitive. Resistive strain-sensitive flexible sensors are flexible tactile sensors that use the resistance-strain gauge as the conversion element.[36] These sensors consist of elastic elements and sensitive units, which can be designed in various structural forms based on specific measurement requirements. The sensitive unit is a transducer that converts strain (dimensional changes) on the engineering component into resistance changes. Deformation in the sensitive unit results in varying degrees of contraction or expansion in different regions, causing the internal conductive material to become denser or sparser, leading to changes in the conductive pathway structure (Fig. 2b). This ultimately manifests as a decrease or increase in overall resistance. This relationship can be expressed by the formula:

$$R = \frac{\rho l}{S} \quad (1)$$

where R is the resistance value of the sensitive element (Ω), ρ is the resistivity of the sensitive element (Ω m), l is the length of the sensitive element (m), and S is the cross-sectional area of the sensitive element (m^2).

Compared to traditional resistive strain sensors, resistive strain-sensitive flexible sensors offer increased flexibility due to the choice of flexible materials. This allows the attached sensitive unit to undergo greater deformation under smaller strain forces when the elastic element is deformed by applied

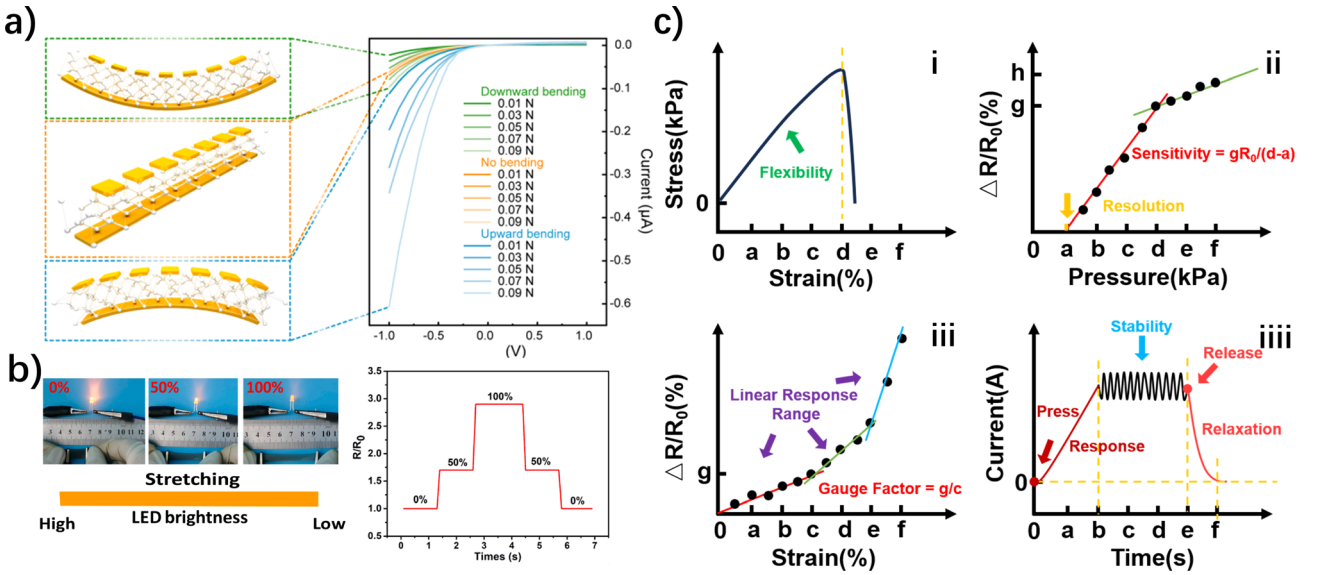

Fig. 2 Principles of flexible resistive tactile sensors. (a) Principle of flexible piezoresistive sensors. The lattice changes under different degrees of bending, resulting in a change in resistance.[35] Reproduced with permission. Copyright at *Nano Energy*, 2022 (b) principle of resistance-strain flexible sensors. Different deformations after applying different external forces lead to changes in resistance, which is externally manifested as a change in the brightness of LEDs.[37] Reproduced with permission. Copyright at *Composites Part A: Applied Science and Manufacturing*, 2022 (c) six key performance parameters of flexible resistive tactile sensors.

force. Consequently, these sensors have higher transmission capabilities. The sensitive unit then converts this deformation into changes in resistance values, making it possible to measure various physical quantities such as pressure, stress, acceleration, and temperature.

The difference between pressure-sensitive flexible sensors and resistive strain-sensitive flexible sensors lies in how resistance changes with pressure. In the former, the change in resistance primarily depends on resistivity variations, while in the latter, resistance changes mainly depend on geometric dimensional changes (strain).

2.2. Performance parameters of flexible resistive tactile sensors

The performance parameters of flexible resistive tactile sensors, such as flexibility, sensitivity, resolution, stability, linear response range, response and relaxation time, *etc.*, can reflect the performance and excellence of the sensor intuitively (Fig. 2c). These indicators are extremely important, and will affect the sensor's operating environment and limit state to varying degrees. Flexible resistive tactile sensors with excellent performance tend to strike a balance between these indicators.

2.2.1. Flexibility. For flexible resistive tactile sensors, their most significant characteristic is their deformability. As shown in Fig. 2c(i), when the strain of the sensor exceeds the limit point d, it will fracture due to overstretching and the force generated will drop dramatically. Thus, scholars typically use strain range and elongation at break to evaluate their flexibility.

Strain ε is usually expressed using the following formula:

$$\varepsilon = \left(\frac{L - L_0}{L_0}\right) \times 100\% \quad (2)$$

where L represents the length of the tactile sensor after deformation (m), and L_0 represents the original length of the sensor (m).

The strain range refers to the maximum deformation range of the flexible resistive tactile sensor without fracturing while maintaining its sensing performance. The strain at which the flexible resistive tactile sensor fractures is referred to as the elongation at break ε', and its formula is as follows:

$$\varepsilon' = \left(\frac{L_{max} - L_0}{L_0}\right) \times 100\% \quad (3)$$

where L_{max} represents the maximum length of the flexible resistive tactile sensor after being stretched (m), and L_0 represents the original length of the sensor (m).

In flexible resistive tactile sensors, flexibility primarily depends on the elasticity of the substrate material, such as polydimethylsiloxane (PDMS), polyethylene terephthalate (PET), polyurethane (PU), and copolyesters (Ecoflex). Additionally, methods such as reducing sensor thickness, decreasing the sensor's Young's modulus, and optimizing sensor structural design can all enhance the flexibility of flexible resistive tactile sensors.[38,39]

2.2.2. Sensitivity. Scholars often use sensitivity (S) to evaluate the sensing performance of flexible resistive tactile sensors, which is represented by eqn (4):

$$S = \frac{R - R_0}{X} \quad (4)$$

For instance, in Fig. 2c(ii), we can use the pressure change (d–a) in the section from a to d with its corresponding resistance change to calculate the sensitivity of the section. Furthermore,

the sensitivity factor (K) can be used to describe the sensor's sensitivity. It reflects the degree of change in the output response of the sensor under a unit input, as shown in eqn (5):

$$K = \frac{R - R_0}{R_0 X} \tag{5}$$

where in eqn (4) and (5), R represents the physical response of the sensor after applying stimulation, R_0 represents the initial physical quantity of the sensor, and X represents the magnitude of the stimulation applied to the sensor.

In addition to sensitivity, scholars also use the relationship between strain and resistance changes in flexible resistive tactile sensors to describe their sensitivity, which is referred to as the Gauge Factor (GF). The expression for GF is as follows:

$$\mathrm{GF} = \frac{R - R_0}{R_0 \varepsilon} \tag{6}$$

where ε represents the strain experienced by the sensor (%), R represents the physical response of the sensor under ε strain (Ω), and R_0 represents the initial physical quantity of the sensor (Ω). In Fig. 2c(iii), the GF of the segment from 0 to c can be expressed as g/c.

The sensitive material in flexible resistive tactile sensors is the primary factor determining their sensitivity. Typically, the better the conductivity of the sensitive material, the higher the sensitivity and responsiveness to external stimuli. Among various sensitive materials, those with excellent conductivity include silver nanowires,[40] graphene (Gr),[41] carbon nanotubes (CNTs),[42] and single-crystal silicon (Si).[43] Additionally, sensitivity in flexible resistive tactile sensors can also be improved through methods such as adjusting the quality ratio of conductive fillers, optimizing the structural design of sensitive units, reducing the initial strength of electrical signals, using novel sensing materials, and introducing non-steady small microcracks.

2.2.3. Resolution. Resolution refers to the ability of a flexible resistive tactile sensor to detect the smallest measurable change in the quantity being measured. In Fig. 2c(ii), the input varies slowly from some non-zero value, and it changes resistance only when the pressure applied on the sensor exceeds a. It can be assumed that force sensing before point a has no action effect and the sensor cannot recognize it. Only when the input changes beyond the resolution does the output change. Typically, the resolution at different points within the sensor's full-scale range is not the same. Thus, within the sensor's full-scale range, the smallest change in the input that causes a step change in the output is used as a measure of resolution, often represented as a ratio x/y, where x is the smallest change and y is the full-scale range.

For flexible resistive tactile sensors, to better simulate the human skin's sensitivity to environmental factors like spatial orientation, pressure, and stress, it's necessary to increase their resolution as much as possible. To enhance spatial resolution, scholars often utilize methods like increasing the number of sensor elements, reducing the size of sensor elements, and developing array-based tactile sensors.[44–46] Additionally, in extremely low-pressure and high-pressure environments, the demands for accurately detecting changes in force are also very stringent, necessitating high resolution.

It's important to note that resolution is a more critical parameter than sensitivity. Sensitivity is a relative measure, while resolution directly reflects the sensor's responsiveness to stimuli. Scholars often focus their research on material selection and microstructure design of the sensitive unit to continually improve both the sensor's operating range and its resolution.

2.2.4. Stability. Stability refers to the ability of a flexible resistive tactile sensor to maintain its performance unchanged over time or with an increase in usage. The stability of a sensor can be quantitatively represented by measuring the change that occurs in its metrological characteristics after a specified period of time or a defined number of usage cycles. In segments b to e in Fig. 2c(iii), the output current of the sensor fluctuates in a small range around a fixed value, and the smaller this fluctuation is, the better the stability of the sensor has when it is in operation.

Factors influencing a sensor's long-term stability extend beyond the sensor's own structure and include the sensor's operating environment. Therefore, for a sensor to exhibit good stability, it must also possess strong environmental adaptability. The sensor's inherent environmental adaptability can be improved through both material selection (hydrophobic, corrosion-resistant, friction-resistant materials) and structural design, enabling the sensor to be hydrophobic,[47] oxidation-resistant,[48] and corrosion-resistant,[49] among other qualities.

2.2.5. Linear response range. The linear response range refers to the range within which a flexible resistive tactile sensor can provide well-behaved linear output signals while operating within its working range. Linearity is an important indicator describing the static characteristics of a flexible resistive tactile sensor, assuming the measured input quantity is in a stable state. Under specified conditions, the maximum deviation ($\Delta Y_{\max}$) between the sensor's calibration curve and the fitted line, expressed as a percentage of the full-scale output (Y), is called linearity. A smaller value of σ indicates better linearity, and the formula is as follows:

$$\sigma = \frac{\Delta Y_{\max}}{Y} \times 100\% \tag{7}$$

Additionally, the linearity can also be described using the linear fitting coefficient R^2. A higher value of R^2 suggests better linearity. Assuming there are n responses y_i corresponding to n excitations x_i, the formula for R^2 is:

$$R^2 = 1 - \frac{\sum_{i=1}^{n} (y_i - \hat{y}_i)^2}{\sum_{i=1}^{n} (y_i - \bar{y})^2} \tag{8}$$

where $\bar{y}$ is the average of n responses:

$$\bar{y} = \frac{1}{n} \sum_{i=1}^{n} y_i \tag{9}$$

Often, for flexible resistive tactile sensors with extremely wide response ranges, the linear response range is not

continuous. Depending on their responsiveness, they can be divided into three sections: low-pressure, medium-pressure, and high-pressure. Each section has a different sensitivity. This phenomenon is mainly due to the occurrence of varying degrees of microcracks within the sensitive unit as it deforms, leading to the interruption of internal conductive pathways. This is reflected as different degrees of resistance change within different excitation ranges. As shown in Fig. 2c(iii), the sensor's rate of change of resistance varies significantly from 0 to c, from c to e, and after e, which is characterized by an abrupt change in slope. The three linear response ranges mean that the sensor has three operating intervals. To mitigate the influence of internal microcracks, more flexible materials can be chosen for the flexible substrate, or nano-materials with fibrous[50] or scale-like[51] structures can be selected for the sensitive unit. This helps the sensor maintain its conductive pathways to a greater extent even when microcracks occur.

2.2.6. Response and relaxation time. Response time refers to the time it takes for a flexible resistive tactile sensor to react to an external stimulus, specifically the time required for the sensor to convert the input stimulus signal into a stable output electrical signal, which is represented in Fig. 2c(iiii) as the time period from 0 to b. A shorter response time allows for more immediate observation of changes in the stimulus level, indicating better dynamic detection performance of the sensor.

Relaxation time, on the other hand, is the time it takes for a flexible resistive tactile sensor to return to a steady state after the removal of an external stimulus. It represents the time it takes for the transient response of the sensor's output electrical signal to settle after the removal of the stimulus signal, which is represented in Fig. 2c(iiii) as the time period from e to f. Relaxation time can characterize the extent of the influence of fast variables. A shorter relaxation time indicates that fast variables are more easily eliminated or reduced.

3. Design and construction of flexible resistive tactile sensors

The diverse performance parameters of flexible resistive tactile sensors are intricately linked to the materials chosen and the structural design employed. As previously discussed, the selection of substrate materials plays a critical role in determining the flexibility of flexible resistive tactile sensors. Sensitive materials primarily govern their sensitivity, linear response range, and resolution, while the structural design exerts a significant influence on the sensor's overall performance. Consequently, investigating flexible substrate materials, conductive sensitive materials, structural design, and performance enhancement remains a significant research direction.

3.1. Flexible substrate materials

Flexible substrate materials encompass the foundational materials that house the conductive sensitive elements in flexible resistive tactile sensors, making up a significant portion of the sensor's composition. The flexibility of flexible resistive tactile sensors is largely determined by the flexible substrate material. This is mainly reflected in aspects such as the sensor's stretch range, Young's modulus, tear strength, hardness, and density, all of which indicate the sensor's deformability to varying degrees. Furthermore, for the purpose of emulating human skin and considering aesthetic factors, researchers often opt for materials that closely resemble the modulus and high transparency of human skin.[52,53] Table 1 presents a performance comparison of several key flexible substrate materials.

There are many substrate materials available for flexible resistive tactile sensors, roughly categorized into rubber, plastic, and fibers. Among them, rubber materials commonly used include PDMS,[54] Ecoflex,[55] and epoxy resin (EP).[56] PDMS is a polymer known for its main chain structure composed of Si–O–Si bonds, providing 100% transparency, along with properties such as heat and cold resistance, hydrophobicity, excellent shear resistance, low stiffness (~2 MPa) and a high thermal expansion coefficient ($\alpha = 310 \times 10^{-6}$ K^{-1}). Tai utilized the thermal expansion property of PDMS to create programmable thermal capabilities in sensors.[57] The value of the real/imaginary part of the impedance of this sensor increased from 10^4 to 10^5 ohms (25 °C) to more than 10^9 ohms (65 °C) at different temperatures, demonstrating its excellent temperature sensing capability (Fig. 3a and b). Ecoflex is a member of the

Table 1 Performance comparison of different flexible substrate materials

Type	Material	Young's modulus	Mechanical strength	Flexibility	Reference
Rubber	PDMS (normally cured high-molecular-weight)	73 kPa to 2.1 MPa	$F_S = 1.5$ MPa	$\varepsilon_{max} = 300\%$	54 and 73
	Ecoflex	50 kPa to 200 kPa	$F_S = 0.3$–0.9 MPa	$\varepsilon_{max} = 860\%$ (Ecoflex 00–50)	55
	EP	2.5 GPa to 5 GPa	$F_S = 0.2$ MPa	$\varepsilon_{max} = 54.2\%$	56 and 74
Plastic	PET	2 GPa to 4 GPa	$F_S = 62$ MPa	$\varepsilon_{max} = 6\%$	61
	PVA fiber	40.02 GPa	$F_S = 1.73$ GPa	$\varepsilon_{max} = 2.88\%$	62
Fiber	Kevlar fibers	70.5 GPa (Kevlar 29/ Longitudinal)	$F_S = 3.6$ GPa	$\varepsilon_{max} = 5.5\%$	64
	Nonwoven fabrics	—	$F_S = 220$ kPa (fiber density: 0.12 g cm^{-3})	$\varepsilon_{max} = 70\%$	70
	Tissue paper	—	$F_S = 100$ kPa	—	72
Others	PU (medical grade)	(8.5 ± 0.3) MPa	—	$\varepsilon_{max} > 400\%$	75

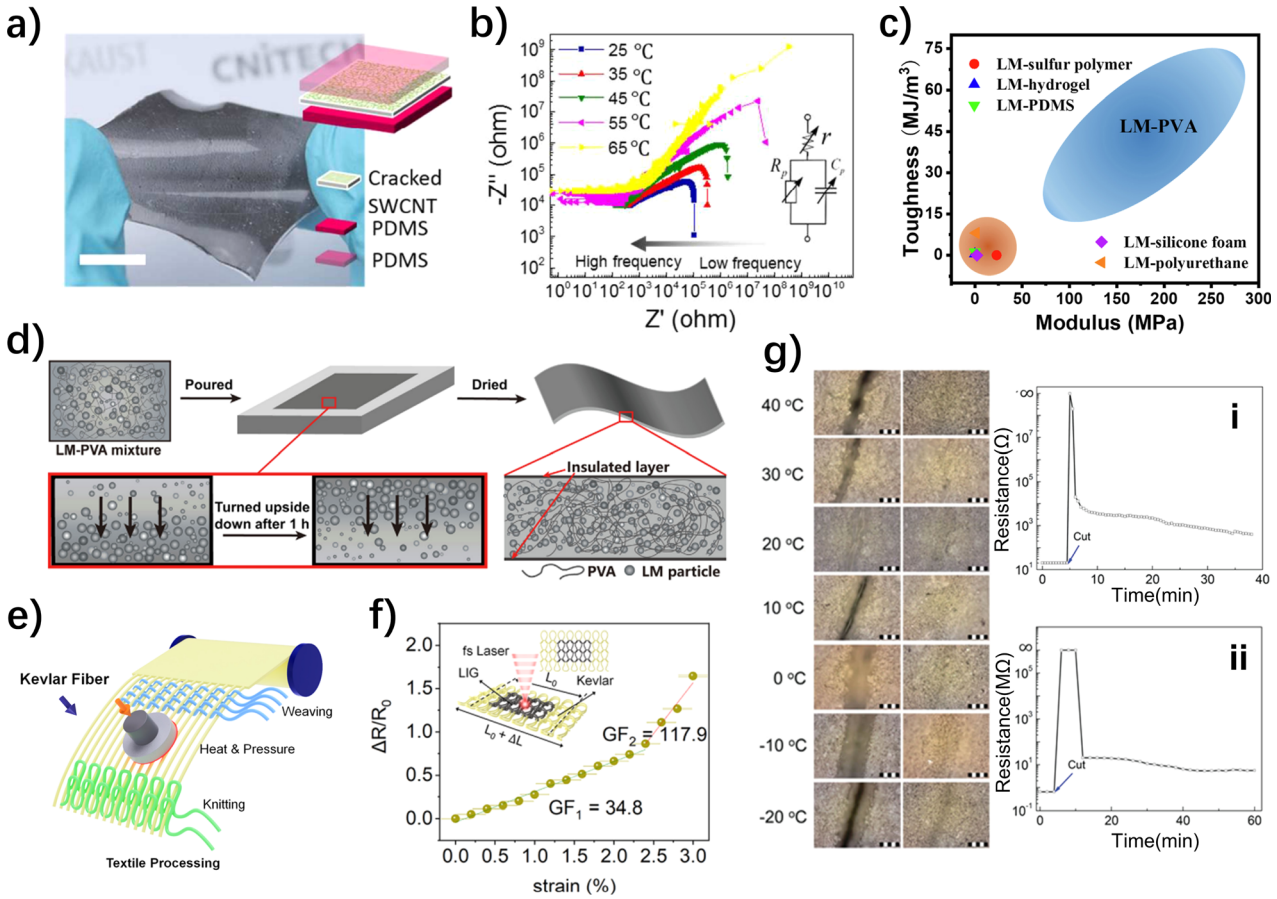

Fig. 3 Structure and performance of different substrate materials for flexible resistive tactile sensors. (a) PDMS is used as a temperature-sensitive flexible material in the substrate.[57] Reproduced with permission. Copyright at *ACS Applied Materials & Interfaces*, 2017 (b) electrical impedance spectroscopies of the sensor at different temperatures from 1 kHz to 2 MHz.[57] Reproduced with permission. Copyright at *ACS Applied Materials & Interfaces*, 2017 (c) mechanical performance of LM-PVA and several other LM-polymer composites.[63] Reproduced with permission. Copyright at *Chemical Engineering Journal*, 2020 (d) scheme for the preparation of LM-PVA film *via* physical blending and drying.[63] Reproduced with permission. Copyright at *Chemical Engineering Journal*, 2020 (e) textile processing with various structures involving Kevlar fibers.[69] Reproduced with permission. Copyright at *ACS Nano*, 2023 (f) sensitivity plots of knit Kevlar/LIG strain sensor at different strains.[69] Reproduced with permission. Copyright at *ACS Nano*, 2023 (g) Images of sh-μAg-PU electrode before cutting and after self-healing at different temperatures: time dependence of logarithmic resistance and healing efficiency of the (i) electrode and (ii) sensing layer.[76] Reproduced with permission. Copyright at *Advanced Materials*, 2016.

super-elastic family, with a fracture strain exceeding 900%. Additionally, its Young's modulus was only 125 kPa, closely matching the Young's modulus of human skin (25–220 kPa), significantly lower than PDMS's Young's modulus. Wang and others utilized nickel nanowires and Ecoflex to fabricate flexible strain sensors with a GF reaching 200 at 100% strain.[58] EP is an organic polymer compound containing two or more epoxy groups. While EP is classified as a type of rubber, it lacks the flexibility seen in materials like PDMS or Ecoflex, demonstrating poor tensile performance, low impact resistance, and a relatively brittle texture. However, EP boasts strong adhesive properties, particularly with metal materials.[59] Based on a screen-printing process, Lin *et al.* prepared a high-performance flexible piezoresistive sensor based on Gr and EP, with response and recovery times of 40.8 ms and 3.7 ms, and a pressure detection range of 2.5–500 kPa.[60] The addition of EP increased the bonding force between the substrate and the conductive material, further expanding the application in sensor.

In plastic materials, PET is widely used due to its linear polymer structure featuring highly symmetrical aromatic rings, which makes it easily orientable and crystallizable.[61] Additionally, PET stands out due to its resistance to folding, creep, fatigue, and friction, coupled with excellent dimensional stability and the highest toughness among thermoplastic plastics. However, its relatively low fracture elongation (150%) and extremely high Young's modulus (4000 MPa) prevented it from being the preferred substrate material. Besides PET, polyvinyl alcohol (PVA) is an excellent water-soluble plastic.[62] Lou *et al.* developed a super-tough force sensor based on liquid metal-polyvinyl alcohol composites (LM-PVA), and the addition of PVA resulted in a dramatic improvement in the toughness and wear resistance of the sensor (Fig. 3d).[63] The sensor exhibited a modulus of elasticity in stress–strain tests that is not found in

most other LM-polymer composites, with a 12.3-fold increase in toughness, and possesses exceptional mechanical durability, remaining stable over 1000 tensile and compressive cycles (Fig. 3c).[63]

Fiber materials have lower flexibility and are not the first choice for electronic skin preparation.[64] However, Kevlar fibers, known for permanent heat resistance, corrosion resistance, high strength, abrasion and tear resistance, unexpectedly caught the attention of scholars.[65–67] Despite its very low fracture elongation (2.8%), Kevlar's advantages in easy processing and material deposition make it a focal point for wearable and protective electronic products. Wang and others deposited shear stiffening polymers (S-ST polymers) and multi-walled carbon nanotubes onto Kevlar to create wearable electronic textiles.[68] The addition of S-ST polymers improved the sensor's impact resistance significantly (dynamic impact resistance increased by 190%). Yang *et al.* transformed pristine Kevlar textiles into conducting laser-induced Gr (LIG) for direct laser writing of e-textiles by using femtosecond laser pulses in ambient air (Fig. 3e). Due to the incorporation of Kevlar fibers, the sensor combined excellent tensile resistance and sensitivity, which changed from 34.8 to 117.9 as the strain increased from 0 to 3.0% (Fig. 3f).[69] Furthermore, affordable and readily available nonwoven fabrics and tissue paper composed of cotton fibers are also favored by scholars. Nonwoven fabric arranges short fibers or filaments in an oriented or random manner to form a fibrous network structure, which was then reinforced using mechanical, thermal, or chemical methods.[70] Liu and others used nonwoven fabric to produce a flexible tactile sensor with a maximum sensitivity of 81.6 kPa^{-1}, a working range of 0–100 kPa, a rapid response time of 6 ms, and a slow response time of 30 ms.[71] Additionally, Pataniya and others coated tissue paper with tungsten diselenide (WSe_2) nanosheets to create a pressure sensor with an ultra-wide pressure working range of 1 Pa to 100 kPa.[72] This sensor exhibited a high sensitivity of 29.24 kPa^{-1} within the pressure range of 1–12 Pa and the capability to detect pressure from small liquid droplets.

Not all materials can be strictly distinguished, and one notable example is PU, which stands out within the superelastic materials category.[77] PU is a block copolymer formed by the polymerization of long and short chain segments, and the properties of PU, such as softness, hardness, and strength, are influenced by the type of segments used.[78] As a result, PU can be produced not only as PU plastics (mainly foam plastics) but also as PU fibers (spandex),[79] PU rubber,[80] and elastomers. PU exhibits exceptional elasticity, with a fracture elongation of up to 800%. Even at 300% elongation, it maintains a rebound rate of over 95%. Moreover, PU possesses flame retardancy, recyclability, and self-healing properties, making it a preferred material for creating self-healing flexible resistive tactile sensors. Huynh and others utilized PU's self-healing ability to develop a self-healing, fully functional, and multiparametric flexible sensing platform which contained the substrate, electrodes, and sensing layer.[76] As shown in Fig. 3g, within a wide temperature range (−20 to 40 °C), the base, electrodes, and chemical resistance of this sensor could fully recover within 16 hours, 30 minutes, and 16 hours, respectively. In addition, both the sensing layer and the electrodes of the platform were able to heal quickly to their original state after being cut.

In addition to the mentioned conventional materials that can serve as flexible substrates, there are also many emerging materials, such as biomimetic materials, showing tremendous potential. In the field of biomimicry material innovation, whether assembling existing materials based on biomimetic structures or directly developing novel biomimetic materials, it can enhance the elasticity and biocompatibility of flexible resistive tactile sensors, achieving more intelligent and biologically analogous sensor responses.[81] Wang *et al.* replicated the anisotropic one-dimensional microstructure of reed leaves, using the multilayer stacking of microgrooved polydimethylsiloxane (*m*-PDMS) to develop a highly sensitive flexible resistive tactile sensor with a sensitivity of 2.54 kPa^{-1}. This sensor achieves a rapid response within 30 ms in a working range of 107 kPa and is applicable in medical and human–machine interaction.[82] Matteo Paolieri and colleagues, inspired by the strong adhesive properties of mussels in the ocean, developed Biomimetic Flexible Electronic Materials using Silk Fibroin-MXene Composites. This material exhibits both high adhesiveness and high stretchability (∼600%) and can be employed in flexible resistive tactile sensors.[83] Additionally, following the principles of biomimicry, we can integrate biomimetic sensing molecules or cell-mimicking materials into sensors to create biomimetic sensing materials. This approach allows for selective sensing of specific stimuli.

In summary, PDMS, Ecoflex, PET, PVA, and PU materials offer notable flexibility and elasticity, making them suitable options for producing highly deformable flexible resistive tactile sensors. EP and PET can serve as substrate materials for sensors that prioritize adhesive properties and friction resistance over extreme flexibility. Biomimetic materials, as novel and advanced materials, have the potential to significantly enhance the performance of substrates. Alternatively, when easy processing and excellent tear resistance are essential, Kevlar and nonwoven fabrics are viable candidates for crafting electronic textiles. It's worth emphasizing that multiple alternative flexible substrate materials exist, each with unique properties, and while this paper offers a broad overview, the selection of materials should align with specific application needs.

3.2. Conductive sensitive materials

The performance of a wide range of parameters in flexible resistive tactile sensors is significantly influenced by the choice of conductive sensitive materials. When coupled with substrate materials that are less flexible, the selection of suitable conductive sensitive materials can empower the sensor to fulfill most requirements and excel in its sensing capabilities.

Commonly used conductive sensitive materials can be broadly categorized into metal-based materials, carbon-based materials, conductive polymers, *etc.* In this context, this paper primarily focuses on metal-based materials such as silver, nickel, gold, copper, and metal compounds. It also discusses commonly used carbon nanocomposite materials like Gr, CNTs, and MXene. Conductive polymers are also frequently utilized in

the conductive layers of flexible resistive tactile sensors, with examples including ionic hydrogels, polypyrrole (PPy), and polyaniline (PANI).

3.2.1. Metal-based materials. Metal-based materials have served as sensitive elements for flexible resistive tactile sensors over an extended period, with researchers frequently working on micro or nano-structuring these materials to meet flexibility demands. These materials are integrated into flexible substrate materials to create conductive networks, allowing the production of a diverse array of flexible resistive tactile sensors while preserving the conductive pathways and deformability.

Silver (Ag), characterized by its exceptional electrical and thermal conductivity, alongside stable chemical properties and remarkable ductility, finds extensive applications and stands out as the most preferred metal-based material. One common approach is to fabricate silver nanowires (Ag NW) or deposit Ag onto other materials to enhance their conductivity.[84] In the conductive pathways formed by silver nanowires, there are three connection states: end-point contact,[85] cross-contact,[86] and non-contact. These different connection states have a significant impact on the formation of conductive pathways and the sensing capabilities of the sensor. Research of Amjadi *et al.* indicated that the more Ag NW deposited on the substrate, the easier it was to form a conductive pathway (Fig. 4a).[87] Consequently, this resulted in a lower initial resistance in the pathway, a broader strain range, and improved linearity (Fig. 4b). However, increasing the thickness of the sensitive layer could lead to a decrease in sensor sensitivity. Therefore, the number and thickness of Ag NW depositions require theoretical consideration and experimental verification. Additionally, despite silver's relatively inert chemical nature, it can react with sulfur-containing substances in the air, which primarily affects silver through sulfidation. To address this issue without compromising the performance of flexible resistive tactile sensors, researchers often embed Ag NW in materials like Gr and reduced Gr oxide to enhance their antioxidation properties.[88]

Nickel is a hard, ductile, and ferromagnetic metal with good oxidation resistance, conductivity, magnetism, and plasticity. Initially, researchers used nickel nanoparticles to fill the

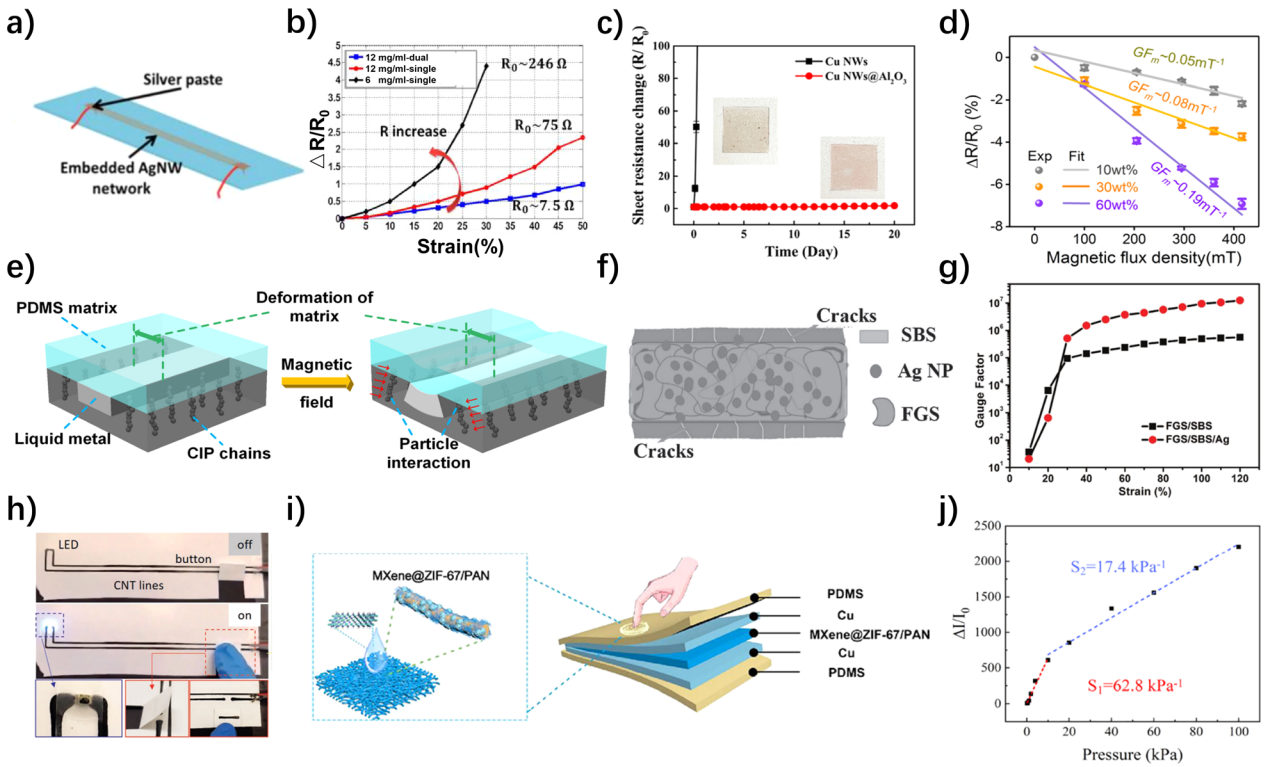

Fig. 4 Structure and properties of the metallic and carbon-based materials based flexible resistive tactile sensors. (a) AgNW is embedded in the sensor's sandwich.[87] Reproduced with permission. Copyright at *ACS Nano*, 2014 (b) relative change of resistance *versus* strain for the sensors with different levels of initial resistance.[87] Reproduced with permission. Copyright at *ACS Nano*, 2014 (c) change in the sheet resistance of pristine Cu NWs network and Al_2O_3@Cu NWs network under ultraviolet ozone irradiation.[91] Reproduced with permission. Copyright at *Chemical Engineering Journal*, 2023 (d) $\Delta R/R_0$ *versus* magnetic flux density.[92] Reproduced with permission. Copyright at *Sensors and Actuators B: Chemical*, 2020 (e) schematic illustration of the magnetic-electric coupling sensing mechanism.[92] Reproduced with permission. Copyright at *Sensors and Actuators B: Chemical*, 2020 (f) structures in sensors filled with FGS conductive layers.[93] Reproduced with permission. Copyright at *Small*, 2017 (g) GF *versus* strain for FGS/SBS and FGS/SBS/Ag composite.[93] Reproduced with permission. Copyright at *Small*, 2017 (h) circuit drawn using carbon nanotube ink. The LED lights up when the switch is closed and the power is on.[94] Reproduced with permission. Copyright at *Advanced Functional Materials*, 2021 (i) schematic illustration of the MXene/ZIF-67/PAN nanofibers and MXene/ZIF-67/PAN film-based pressure sensor.[95] Reproduced with permission. Copyright at *ACS Applied Materials & Interfaces*, 2022 (j) sensitivity curve of this device at 200 Pa to 100 kPa.[95] Reproduced with permission. Copyright at *ACS Applied Materials & Interfaces*, 2022.

substrate material for flexible sensors. However, pure nickel nanoparticles alone did not achieve high-performance sensor metrics. Therefore, methods such as embedding nickel in other polymers, growing gold needle shells on silver-plated nickel nanoparticles and electrodepositing nickel nanoparticles on Gr coatings gradually emerged.[89] Han *et al.* achieved an initial microcrack formation on the metal surface through electrodepositing nickel nanoparticles on Gr, which then generated additional microcracks during the tensile strain process.[90] This dual microcrack mechanism allowed the sensor to achieve a highly sensitive GF value of up to 3360.09 within strain range from 20% to 60%. Furthermore, similar to silver, nickel can also exist in the form of nickel nanowires (Ni NW) in flexible resistive tactile sensors. Wang *et al.* proposed a simple and cost-effective magnetic field-assisted chemical reduction method to fabricate Ni NWs with widths as low as 21 nm and a high aspect ratio (L/D) of up to 300.[58] Surprisingly, the strain sensor fabricated from these Ni NWs exhibited a GF of approximately 200 within the 0% to 100% strain range, indicating good sensitivity. While the strain sensor model may seem relatively uncomplicated, it effectively showcases the potential of Ni NWs in flexible resistive tactile sensor applications.

In addition to silver and nickel, gold, which has high density, excellent conductivity, and good ductility, has also attracted the attention of researchers. However, due to its high cost, gold is mostly added in small amounts to flexible resistive tactile sensors in the form of nanoparticles or nanowires.[96] For instance, Huynh and Haick introduced self-repairing gold nanoparticles into a chemically resistant crosslinked polyurethane base, sandwiched between two layers of silver microparticle polyurethane, resulting in the development of a versatile, flexible sensor possessing the ability to self-heal.[76] The loaded sensitivity of the chemiresistive sensor after cutting remained stable at (0.09 ± 0.01) g F^{-1}. Furthermore, copper nanowires (Cu NW), known for their good conductivity, have also captured researchers' attention. Although Cu NW is more susceptible to oxidation compared to the previously mentioned metal-based materials, addressing the oxidation issue and utilizing Cu NW to fabricate high-performance flexible resistive tactile sensors is of significant importance, particularly in the context of resource scarcity. Whether using quasi *in situ* polymerization, using PDMS as a sealing material to isolate air, or encapsulating Cu NW with other conductive materials, these are viable approaches to address the oxidation issue of Cu NWs. Zhao *et al.* enhanced the thermochemical stability of Cu NWs using solution-grown Al_2O_3 nanoshells.[91] After the covering treatment with Al_2O_3 nanoshells, the Cu NWs maintained a relatively stable resistive resistance value in the comparison experiment for up to 20 days (Fig. 4c).

Besides elemental metals, certain highly conductive metal compounds and liquid metals can also serve as sensitive materials for flexible resistive tactile sensors, displaying impressive performance.[97] Rana *et al.* utilized polycrystalline MoS_2 to fabricate flexible strain sensors that exhibited excellent sensitivity ($GF = 80 \pm 2$) and stability over a wide range of stresses ($\geq$14 MPa).[98] Similarly, Pataniya employed adaptable pressure-sensitive paper devices that were enhanced with WSe_2 nanosheets. These devices showcased an exceptionally broad pressure operating range spanning from 1 Pa to 100 kPa, and achieved the highest sensitivity at 29.24 kPa^{-1}.[72] They demonstrated swift response times of 200 ms and relaxation times of 100 ms, enabling them to detect pressures as minute as 1.4 Pa, such as those generated by water droplets. Additionally, Hu *et al.* employed the liquid metal GaInSn for electronic circuits, creating a magnetoflexible resistive strain sensor with self-healing capabilities (Fig. 4e).[92] When the content of carbonyl iron particles was increased from 10 wt% to 30 wt% and 60 wt%, the absolute value of $GF_m(\frac{\Delta R/R_0}{\Delta B}$, ΔB was the variation of magnetic flux density) was significantly increased, with a corresponding significant increase in magnetic sensitivity (Fig. 4d).

3.2.2. Carbon-based material. It's well known that carbon-based materials encompass materials with excellent conductivity. Unlike metal-based materials, these materials are not constrained by resource availability and are relatively environmentally friendly. Gr, CNT and MXene are particularly strong contenders as conductive sensitive materials.

Gr, a material formed by closely packed carbon atoms in a single-layer two-dimensional honeycomb lattice, exhibits outstanding optical, electrical, and mechanical properties, with a carrier mobility of approximately 15 000 cm^2 $(V\ s)^{-1}$ at room temperature. Researchers often blend Gr with other conductive sensitive materials to enhance the sensing capability of the sensitive layer.[99] Beyond traditional sheet-like Gr, materials like Gr foams and Gr sponges have also gained traction. However, the fabrication process for Gr foams can be complex and costly. To reduce costs and enhance sensitivity, some researchers have sought process improvements. In addition to conventional methods of synthesizing Gr foams *via* vapor deposition, Li *et al.* have developed a simple and scalable self-assembly approach under milder conditions to create high-performance Gr foams.[100] The resulting flexible resistive tactile sensors exhibit advantages such as high tensile sensitivity and good reproducibility. Likewise, Gr sponges offer exceptional performance. For instance, Zhao *et al.* employed fragmentized Gr sponges (FGS) to fabricate high-performance sensors (Fig. 4f).[93] Gr sponges are porous three-dimensional networks composed of interconnected graphene sheets, while FGS refers to graphene sponges that have been fragmented into micro-sized structures. Sensors crafted from FGS exhibited remarkable electrical conductivity (1521 S cm^{-1}) along with impressive mechanical properties, displaying a fracture elongation of 680% and a tensile strength of 3.5 MPa. Upon doping FGS with polystyrene-butadiene-block styrene (SBS) and silver (Ag) nanoparticles, they displayed extraordinarily high sensitivity. The GF increased from 20.5 at 10% strain to 1.25×10^7 at 120% strain (as shown in Fig. 4g). Additionally, these sensors demonstrated rapid response times of less than 20 ms and maintained excellent stability throughout tests surpassing 2000 cycles.

CNTs are primarily composed of layers of carbon atoms arranged in a coaxial cylindrical tube structure. As one-dimensional nanomaterials, CNTs are lightweight and exhibit a seamless hexagonal structure, resulting in exceptional

mechanical, electrical, and chemical properties. In the field of flexible resistive tactile sensors, CNTs are often integrated with diverse materials to create sensing units, and these combinations may involve materials such as graphite nanoplatelets (GNPs), LIG, or carbonyl iron powder, contributing to improved sensing performance.[101] CNTs can also be integrated with shear-thickening gels (STGs) or shear-stiffening (S-ST) polymers to impart impact resistance.[102] Furthermore, with the emergence of 3D printing technology, some researchers have utilized novel CNT inks to fabricate flexible pressure-sensitive sensors through 3D printing. Owens *et al.* introduced a polymer-free, water-based ink containing carbon nanotubes that can be printed (Fig. 4h).[94] This ink allowed for the creation of a conductor with a conductivity of up to 10 000 S m^{-1}. It exhibited outstanding flexibility and stability, with a DC resistance change of less than 5% after undergoing 1000 bends. Additionally, the DC resistance changed by less than 3% when the bend radius was less than 1 mm. This printing technology holds the potential to lower manufacturing costs for wearable sensors, radio-frequency identification (RFID) tags, and deformable structures.

MXene is a new class of inorganic two-dimensional materials, meaning layered transition metal carbides or nitrides, and possesses a structure similar to Gr. Within the family of MXene materials, the carbon-containing branches are frequently integrated into other materials, serving as a significant component of carbon-based materials. Also, due to the hydroxyl group or terminal oxygen on the surface of their materials, they stand out among many materials by virtue of their extraordinary transition metal carbide conductivity and flexibility, making them promising conductive materials for flexible resistive tactile pressure sensors.[103–105] Li *et al.* developed a highly conductive MXene-based organohydrogel (M-OH) based on Ti_3C_2Tx MXene/lithium salt (LS)/polyacrylamide (PAM)/PVA hydrogel, which achieved 2000% stretching and excellent conductivity of 4.5 S m^{-1}.[106] The addition of MXene resulted in the dramatic increase in the electrical conductivity of the material. Due to the agglomeration effect of MXene in the supersaturated state, they finally found a balance between electrical conductivity and mechanical properties at a concentration of 1.0 wt%. Besides, Zhang *et al.* designed a flexible and conductive MXene/PEDOT:PSS@Melamine Foam (MPMF) piezoresistive sensor with a stabilized coating that combined excellent mechanical properties and electrical conductivity, and a wide operating range of the material that allowed it to generate up to 80% of the compressive strain at a pressure of 60 kPa, with good sensitivity (0.30 kPa^{-1}) and a wide linear working region (12–60 kPa).[107] Similarly, Fu *et al.* developed a device based on MXene/ZIF-67/PAN films (Fig. 4i).[95] Although its linear response range (0.2–10 kPa, 20–100 kPa) was not as uniform as the previous one, it had a superb sensitivity (62.8 kPa^{-1}) and strong mechanical stability (more than 10 000 loading/unloading cycles), enabling the long-term wear and health monitoring (Fig. 4j).

Of course, apart from Gr, CNTs, and MXene, some researchers are exploring how to use low-cost carbon-based material to create high-performance flexible resistive tactile sensors. Liu *et al.*, for example, employed a vapor deposition method to uniformly coat carbon black (diesel soot) onto textiles, resulting in a flexible pressure sensor.[71] This sensor also exhibited significant sensitivity and operating range, demonstrating practical applications in sound signal monitoring and human physiology, including the detection of subtle pulse vibrations.

3.2.3. Conducting polymers. Many conductive polymer materials play a crucial role in the sensitive materials of flexible sensors due to their flexibility and good conductivity. Among these materials, widely studied ones include PPy,[108] PANI,[109] and more. Sensors fabricated from these materials have achieved remarkable results, such as ultrahigh sensitivity reaching 46.48 kPa^{-1} within the range of 0 to 4.5 kPa, and even the ability to monitor the placement and removal of tiny masses, for instance, detecting extremely low pressures of 0.8 Pa corresponding to a petal.[110,111] Furthermore, to attain specific functionalities, some researchers introduced other materials by doping them into conductive polymer materials. For instance, Wang *et al.* developed a novel multifunctional sensor with a multilayered internal three-dimensional network structure using collagen aggregate from chromium-containing waste leather, PANI, and acidified MWCNT.[112] This sensor exhibited a tensile GF of 5.2, a bending GF of 9.2, and a dynamic response range from 28 Pa to 100 kPa.

In recent years, Poly(3,4-ethylenedioxythiophene):Poly(styrene sulfonate) (PEDOT:PSS) has become one of the most desirable materials for the preparation of flexible resistive tactile sensors due to its excellent electrical conductivity, mechanical flexibility and ease of processing.[113–115] This material is often made into thin films or doped into other conductive polymers to provide additive good electrical and mechanical properties for piezoresistive sensors.[116–118] Xia *et al.* created a mild treatment with formamide and methanol as co-solvents to optimize the conductive properties of PEDOT:PSS films.[119] Due to the high dielectric constant and hydrophilicity of formamide and the solvation of methanol, the insulating PSS could be separated from the PEDOT, leading to a significant increase in the film conductivity of PEDOT:PSS from 0.3 to 1287 S cm^{-1}. Beccatelli *et al.* functionalized PU foams by using PEDOT:PSS to propose a modified all-polymer foam (Fig. 5a).[120] This material, due to its excellent linear response range (0–30 kPa, 30–50 kPa) and high sensitivity, was applied to a prototype insole with eight pressure sensors, which could be used for medical rehabilitation and professional data monitoring of athletes (Fig. 5b). To enhance the adhesion and practicality of PEDOT:PSS, scholars modified the substrate material and optimized its structure, as PEDOT:PSS typically requires attachment to a substrate for utilization.[121,122] Lee *et al.* used ultrafiltration to exchange water-based PEDOT:PSS solution for organic solvent-based PEDOT:PSS solution.[123] After optimization, PEDOT formed a stable and sensitive thin nano-coating on the surface of hydrophobic pyramid-type PDMS with good bonding. Yang *et al.* deposited the PEDOT:PSS solution on a thin sheet of paper, and used the paper's fiber microstructure to design stacked and folded structures with good binding to PEDOT:PSS (Fig. 5c).[124] Based on the extrusion and expansion between the

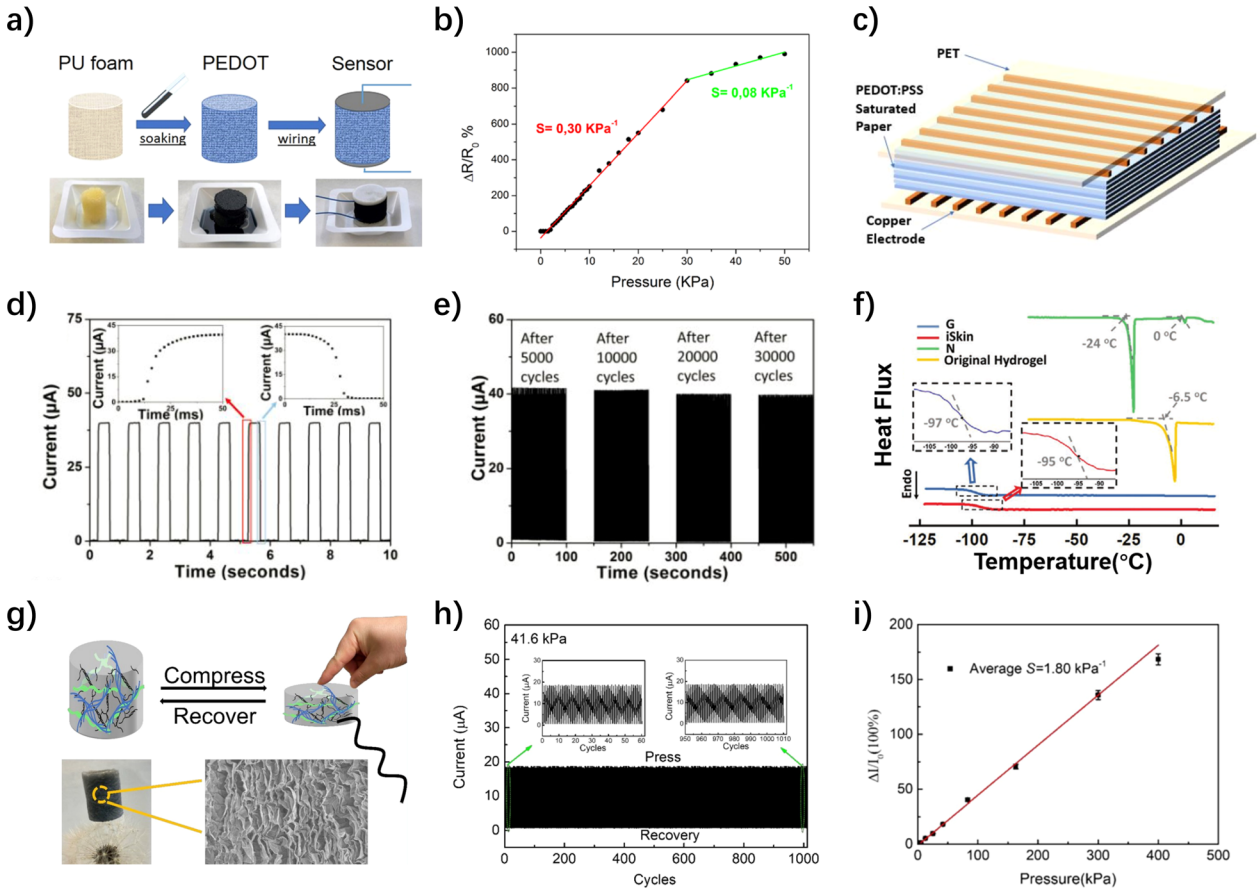

Fig. 5 Structure and performance of flexible resistive tactile sensors based on conducting polymers and conductive hydrogels. (a) Pictorial illustration of the fabrication process of the pressure sensitive all-polymeric device.[120] Reproduced with permission. Copyright at *ACS Applied Polymer Materials*, 2021 (b) sensor response as a function of external pressure.[120] Reproduced with permission. Copyright at *ACS Applied Polymer Materials*, 2021 (c) schematic of a 7 × 7 pixel pressure sensor made by sandwiching 8 layers of PEDOT:PSS-saturated paper between two PET substrates with crossed arrays of copper electrodes.[124] Reproduced with permission. Copyright at *ACS Applied Materials & Interfaces*, 2019 (d) the response kinetics upon application and release of pressure.[124] Reproduced with permission. Copyright at *ACS Applied Materials & Interfaces*, 2019 (e) current response for 100 load/unload cycles, recorded after 5000, 10 000, 20 000, and 30 000 cycles.[124] Reproduced with permission. Copyright at *ACS Applied Materials & Interfaces*, 2019 (f) dynamic scanning calorimetry (DSC) results at the endo direction of iSkin and other materials.[132] Reproduced with permission. Copyright at *Advanced Functional Materials*, 2021 (g) protein nanofibers can be used to improve the mechanical properties of gelatin aerogels and increase their elasticity.[133] Reproduced with permission. Copyright at *ACS Applied Bio Materials*, 2022 (h) current–time (*I*–*t*) curves of the sensor when repeatedly applying and removing a weight corresponding to a pressure of 41.6 kPa (1000 cycles).[133] Reproduced with permission. Copyright at *ACS Applied Bio Materials*, 2022 (i) average sensitivity of five independently prepared LPNF : GEL : PEDOT-S (2.7 : 8 : 1) aerogels.[133] Reproduced with permission. Copyright at *ACS Applied Bio Materials*, 2022.

paper layers, the stacked paper sensor has a sensitive response (less than 20 ms) and superb durability (more than 30 000 loading and unloading cycles) (Fig. 5d and e). On the manufacturing side, in addition to being synthetic, the highly conductive, chemically stable, and translucent PEDOT:PSS is also machine-printable, which greatly contributes to sensor material savings and cost reductions.[125,126]

In response to the current resource scarcity, researchers have been exploring new types of conductive polymer materials for sensor fabrication. Yin *et al.* investigated the use of "green" renewable resource cellulose nanofibers (CNF) to create multi-functional flexible sensors.[127] They mixed CNF with Ag NW to produce composite films, which were then sandwiched between two layers of thermoplastic polyurethane (TPU) to create flexible sensors capable of detecting strain and temperature. After a 10% pre-strain treatment, this sensor achieved a GF of 34.06 at a strain of 1.5%, and it was capable of detecting strains as low as 0.2%. It demonstrated good detection abilities in measuring pulses, vocal cord vibrations, and finger bending. Additionally, the sensor exhibited effective temperature-sensing behavior in response to changes in external temperature.

3.2.4. Conductive hydrogels. Conductive hydrogel, known for its excellent electrical and mechanical properties, melds the conductivity of rigid metals with the fluidity of liquids, and it is frequently employed in semi-dry electrodes.[128] Researchers have undertaken diverse optimization strategies, including refining the manufacturing process and incorporating high-toughness, high-conductivity materials, to consistently enhance the performance of conductive hydrogels. Guo *et al.* used poly-acrylamide (PAM) and sodium carboxymethyl cellulose

(CMCNa) as raw materials to prepare a new type of double-network (DN) organic hydrogel with high tensile strength (~0.9 MPa), elongation at break (~1097%), and toughness (~4.75 MJm^{-3}) by photoinitiated polymerization, transition metal ionic complexation and solvent exchange, and the ionic conductivity is 0.107 S m^{-1}.[129] In contrast, the ion-conducting nanocomposite hydrogel developed by Wu *et al.*, with the addition of minute quantities of carbon nanotubes, exhibited significantly enhanced mechanical properties, boasting a tensile strength, elongation at break, and toughness reaching 1.09 MPa, 4075%, and 12.8 MJ m^{-3}, respectively.[130] The electrical conductivity was dramatically improved after LiCl doping, and the ionic conductivity was up to 0.85 S m^{-1}.

Conductive hydrogel, despite its advantages, faces challenges related to environmental sensitivity, self-healing limitations, rigidity, and power requirements, necessitating careful material and structural design choices. By incorporating hygroscopic and cryoprotective substances, it is possible to mitigate water loss, thereby diminishing the temperature and humidity susceptibility of hydrogels to some extent.[131] Taking cues from human skin attributes, Ying *et al.* developed an innovative ionic skin using a novel viscous hydrogel formulation containing glycerol and concentrated salts, which resulted in a material exhibiting exceptional resistance to low temperatures (−95 °C) while possessing an elongation at break of 1975% with a conductivity of 0.904 S m^{-1} (Fig. 5f).[132] Dai *et al.* designed a dual physically and chemically crosslinked triple-network hydrogel (PVA/B TN hydrogel), which improved the mechanical properties of this type of hydrogel and demonstrated superb self-healing ability at room temperature (healing time of 5 min, healing efficiency of 98.1%).[134] Fu *et al.* designed a high-strength, self-powered piezoelectric polyacrylonitrile-polyvinylidene fluoride (PAN-PVDF) hydrogel. In the working system, they used PVDF as a self-powered source due to its piezoelectricity and excellent plasticity.[135] The hydrogel sensor provided a consistent and steady electrical signal output in response to mechanical stimulation (~30 mV and ~2.8 μA), and it exhibited a rapid response time of ~31 milliseconds. This allowed it to effectively translate alterations in the hydrogel's electrical resistance caused by an external force into changes in voltage output signals, all without requiring an external power source.

Aerogels and hydrogels share gel-like characteristics, yet unlike the constraints associated with hydrogels, aerogels have adeptly circumvented water loss issues through their robust physical attributes and exceptional environmental resilience, establishing themselves as a promising alternative. Wang *et al.* prepared a highly flexible and compressible aerogel with a smooth layer structure by compounding silver nanowires with PEDOT:PSS and polyimide.[136] Within the constraints of the dispersing medium's limits, this aerogel exhibited impressive sensitivity (0.31 kPa^{-1}). In contrast, hydrogels are susceptible to negative effects within the range of 0–1.25 kPa. Moreover, the aerogel's compressive strain showed remarkable synchronization with the rate of change in electrical resistance, achieving an astonishing linearity of 1, underscoring its exceptional sensing capabilities. Aerogels exhibit significantly reduced flexibility due to their lower water content compared to hydrogels. In order to improve its elasticity and flexibility, Yuan *et al.* proposed an innovative scheme by mixing lysozyme PNFs (LPNFs), gelatin, and leaving it to self-assemble to form a protein nanoproto-fiber, while adding poly(4-(2,3-dihydrothieno[3,4-*b*]-[1,4]dioxin-2-yl-methoxy))-1-butanesulfonic acid (PEDOT-S), which could improve the strength of the gel.[133] After undergoing a process involving freezing, decompression, and evaporation, the mechanical properties of the mixture showed a significant enhancement (Fig. 5g). The modified aerogel exhibited remarkable electrical attributes. It displayed consistent and swift current responses even after undergoing more than 1000 cycles of load and unload tests. Additionally, it demonstrated a clear linear correlation across a wide pressure range from 1.8 to 300 kPa, and maintained an average sensitivity of 1.80 kPa^{-1}, positioning it as a highly promising material for piezoresistive pressure sensors (Fig. 5h and i).

There are also advanced two-dimensional materials or composite materials that can be used as conductive materials. In addition to graphene, 2D materials such as indium selenide (InSe), molybdenum disulfide (MoS_2), and others exhibit high electron mobility and good mechanical flexibility, making them suitable for manufacturing highly sensitive tactile sensors. Chen *et al.* developed a flexible, ultra-sensitive three-terminal strain sensor based on two-dimensional (2D) InSe, which can be used to detect human movement.[137] InSe greatly enhances the current change, resulting in an 8-fold increase in the GF of the sensor under 0.25% tensile strain, reaching 32. Pang *et al.* successfully grew amorphous MoS_2 on a 1.5 μm thick PDMS substrate through magnetron sputtering. They designed and fabricated a micro-thin film flexible sensor.[138] At a pressure of 0.46 MPa, the maximum $\Delta R/R$ is 70.39, with a high piezoresistive coefficient of 866.89 MPa^{-1}. It passed the human foot pressure test, demonstrating enormous potential in medical health. There are many advanced composite materials, such as glass fiber reinforced polymers, nanocomposites, and carbon nanotube reinforced polymers. These composite materials significantly enhance the conductivity of sensors and selectively optimize the weaknesses of conventional flexible resistive tactile sensors. For example, Kang *et al.* prepared a flexible resistive tactile sensor based on graphene-silver nanoplate-polymer nanocomposites.[139] Its sensitivity is 0.04 kPa^{-1}, with a response time of approximately 286 ms. Additionally, it exhibits hydrophobicity and self-cleaning properties, making it suitable for wearable devices. Fu *et al.* prepared a reduced graphene oxide-coated glass fabric/organosilicon composite material (RGO@GF) and used it to manufacture a high-performance structural flexible strain sensor.[140] Glass fibers and silicon resin provide mechanical strength and flexibility, respectively. While adequately protecting the fragile internal structure, the composite material also possesses a gauge factor (GF) value of approximately 113. Furthermore, the addition of graphene imparts conductivity to the glass fibers. Clearly, achieving such comprehensive performance enhancement in composite materials is easily attainable.

Currently, there is a wide variety of conductive sensitive materials used in resistive-type flexible tactile sensors, and they

Table 2 Comparison of the performance of different sensors[a]

Flexible substrate materials	Conductive sensitive materials	Flexibility	Sensitivity	Linear response range	Response and relaxation time	Reference
Ecoflex elastomer	Nickel nanowires	100%	GF = 200	—	0.32 s, —	58
Epoxy resin	Graphene	—	$S_1 = 0.156\ kPa^{-1}$ $S_2 = 0.068\ kPa^{-1}$ $S_3 = 0.023\ kPa^{-1}$	2.5–100 kPa (S_1) 100–250 kPa (S_2) 250–500 kPa (S_3)	40.8 ms, 3.7 ms	60
Liquid metal	Golyvinyl alcohol	540%	$GF_1 = 0.1\ MPa^{-1}$ $GF_2 = 1.2\ MPa^{-1}$ $GF_3 = 0.2\ MPa^{-1}$	0–0.6 MPa (GF_1) 0.6–2.2 MPa (GF_2) 2.2–3.2 MPa (GF_3)	—	63
Knit Kevlar	Laser-induced graphene	3%	$GF_1 = 34.8$ $GF_2 = 117.9$	—	0.192 s, 0.177 s	69
Tissue papers	WSe_2 nanosheets	—	$S_1 = 29.24\ kPa^{-1}$ $S_2 = 11.94\ kPa^{-1}$ $S_2 = 3.20\ kPa^{-1}$	0.001–0.012 kPa (S_1) 2–30 kPa (S_2) 35–100 kPa (S_3)	200 ms, 100 ms	72
Self-healing disulfide-cross-linked polyurethane	Self-healing polyurethane/silver-microparticles composite	97.34%	$GF_1 = 66.11 \pm 16.08$ (normal) $GF_2 = 82.38 \pm 12.10$ (under electrode-cut) $GF_3 = 30.22 \pm 4.14$ (under AuNP-cut)	—	—	76
PDMS elastomer	Silver nanowire	70%	Tunable GF: 2–14	—	200 ms, —	87
PDMS elastomer	Nickel nanoparticles and graphene coated polyurethane sponge	65%	$GF_1 = 36.03$ $GF_2 = 3360.09$	0–20% strain (GF_1) 20% to 65% strain (GF_2)	100 ms, —	90
PET	MoS_2	—	GF = 80 ± 2 (2 μm SU-8 encapsulated)	Stress ≥14 MPa	—	98
Poly(styrene-block-butadiene-block-styrene)	Fragmentized graphene sponges and Ag nanoparticles	680%	Tunable GF: 20.5–1.25×10^7 (strain: 10–120%)	—	20 ms, —	93
Melamine foam modified with polydopamine	Mixture of MXene and PEDOT:PSS	80% (compression strain)	$S = 0.30\ kPa^{-1}$	12–60 kPa	200 ms, 120 ms	142
Commercial polyurethane	PEDOT:PSS	—	$S_1 = 0.30\ kPa^{-1}$ $S_2 = 0.08\ kPa^{-1}$	0–30 kPa (S_1) 30–50 kPa (S_2)	—	120
Hydrogel	MWCNTs	4075%	$S_1 = 0.062\ kPa^{-1}$ $S_2 = 0.022\ kPa^{-1}$ $S_3 = 0.008\ kPa^{-1}$	0–5 kPa (S_1) 5–9 kPa (S_2) 9–15 kPa (S_3)	0.18 s, —	130
Gelatin and lysozyme protein nanofibrils	PEDOT-S	—	$S = 1.8\ kPa^{-1}$	1.8–300 kPa	—	143

[a] Tip: definitions of sensitivity expressions for sensors may vary across different articles. This table uses both GF and S parameters to describe sensor sensitivity. The definitions of GF and S can be found in the second section of this article.

are not limited to the aforementioned categories of metal-based materials, carbon-based materials, conductive polymers, and hydrogels. The performance specifications of flexible resistive tactile pressure sensors with different substrate and conductive sensitive materials are shown in Table 2. In summary, when fabricating resistive-type flexible tactile sensors, researchers often choose flexible substrates like PDMS, PET, PU, Ecoflex, and excellent conductive materials like Ag NW, Gr, CNT, PEDOT, MXene, conducting hydrogels, *etc.*, as sensitive materials. The combination of these materials has led to the development of various high-performance sensors, demonstrating excellent performance in stretchability, sensitivity, and linearity.[141]

3.3. Sensor structure design and performance optimization

The design of sensor structures and performance optimization are widely acknowledged as critical factors that greatly affect various performance parameters in flexible resistive tactile sensors. The flexibility, sensitivity, and stability of the sensor are directly influenced by its structural design, which is essential for fully utilizing the potential of the materials.[144] Additionally, to improve sensor resolution, detect three-dimensional forces, and meet the integration requirements of flexible electronic skins, researchers often choose to incorporate unit arrays into flexible resistive tactile sensors. By employing multi-point monitoring methods and utilizing sensor calibration and decoupling techniques, they can achieve multifunctional and highly precise sensing.

3.3.1. Sensing unit and microstructure design. The early concepts of flexible resistive tactile sensors commonly utilized a "sandwich" configuration, a design choice that gained widespread acceptance for its straightforwardness and efficiency. This sandwich structure entails the use of a flexible substrate material as the outer layer and the incorporation of a conductive sensing material as the inner layer.[58] This configuration adeptly shields the sensor's sensitive layer, safeguarding it from potential harm in intricate external conditions. Additionally, when subject to bending and stretching, the fractured and flexed sensitive layer can reestablish connections as the upper and lower encapsulation layers regain their original form, ensuring the continuity of sensing functionality.[87] Consequently, the sandwich structure imparts good repeatability, reliability, stability, and extended lifespan to the sensor. Of course, apart from the layered configuration, researchers also design sandwich structures in various forms like linear or columnar arrangements to cater to specific applications.[145]

However, the simple sandwich structure alone may not meet the requirements of flexible resistive tactile sensors for high precision and sensitivity. Therefore, many researchers have enhanced the sensing performance by optimizing various microstructures based on the sandwich structure.[146] Generally, microstructure design can be roughly categorized into surface microstructures and internal microstructures. Surface microstructures involve creating features such as curved folds,[147] cone-like structures,[148] hemispherical structures,[149] interlocking structures,[150] and biomimetic structures[151] on the substrate surface. These structures increase the contact area between the substrate and the sensing unit, thereby enhancing the sensitivity. Internal microstructures, on the other hand, entail constructing features like porous structures, interlocking structures, and biomimetic structures within the flexible substrate or the sensing unit itself. These internal spatial arrangements, such as gaps between adjacent frameworks or hollow channels within the framework, can increase the contact area and decrease the contact resistance of the sensor when subjected to external forces.[152]

Among the surface microstructures, one of the relatively easier designs is the surface curvature and folding structure. Kim *et al.* introduced a serpentine pattern that allowed for diverse responses to different stresses through curvature control.[153] Smaller curvature serpentine strips were found to exhibit greater strains under the same stress when compared to their larger curvature counterparts. The design with larger curvature is better for reducing induced strain and high-stress monitoring, while the design with smaller curvature provides higher sensitivity, reaching 0.41% kPa^{-1} within the 0% to 10% strain range, capable of detecting pressures as low as 0.87 kPa. Conversely, the design with larger curvature provided a wider linear working range, offering a sensitivity of 0.075% kPa^{-1} within the 0% to 30% strain range. Additionally, Xiang *et al.* utilized the rough structure of sandpaper, coated it with PDMS and Alk-Ti_3C_2, to create a flexible pressure-sensitive sensor with surface folding (Fig. 6a).[154] The implementation of this structure resulted in a notable enhancement of sensitivity across the operating range of 0–800 kPa. More precisely, it exhibited a sensitivity of 95.26 kPa^{-1} in the low-pressure range of 0–1 kPa and a sensitivity of 543.66 kPa^{-1} in the high-pressure range from 200 to 600 kPa (Fig. 6b). Surface biomimetic structures and interlocking structures can also provide excellent performance to sensors.[155] Although both often involve technologies like 3D printing and UV exposure, which pose challenges in terms of construction difficulties and technical complexity, their high sensitivity and reliability have still led many researchers to conduct extensive studies in this area. For instance, Chun *et al.* developed a flexible piezoresistive sensor with high adhesion and water-resistant stretchability by inscribing octopus-like patterns (OPs) on carbon-based conductive polymer composite (CPC) films (Fig. 6c).[151] The sensor possessed good stability with an estimated sensitivity (S_1) of 0.14% kPa^{-1} by linear fitting for vertical pressure values below 60 kPa, and an improved sensitivity (S_2) of 0.01% kPa^{-1} when the pressure increased from 60 kPa to 1000 kPa (Fig. 6d). Particularly, flexible tactile sensors based on interlocking structures exhibit significant potential. When interlocking fibers come into contact under external force, they deform slightly starting from the tip. The greater the external force, the tighter the interlocking between the fibers, and the more pronounced the deformation becomes. These minor distortions generated by the contact between interlocking fibers can significantly enhance the sensor's sensing ability, allowing it to detect extremely low pressures. Lu *et al.* proposed a new method to prepare highly sensitive flexible pressure sensors using interlocking nanocone arrays (IOCA) (Fig. 6e).[156] Under different pressures, the IOCA squeezed each other due to the interlocking structure, and the height and contact area between the cells changed, which in turn led to the change of IOCA conductivity and affected the pressure sensitivity. The theoretically derived results in Fig. 6f were in high agreement with the experimental results, confirming the rationality of the interlocking structure and the high sensitivity of the sensor. Pang *et al.* utilized interlocked nanofiber arrays coated with platinum to fabricate a sensor capable of detecting extremely low pressures, approximately around 5 Pa. It could also discern shear stress as low as 0.001 N (with a sensing limit of about 1 N), and torsional loads as small as 0.0002 N m.[159] Additionally, within the strain range of 0% to 5%, it exhibited gauge factors of roughly 11.5 for pressure, 0.75 for shear, and 8.53 for torsion. This sensor proved adept at detecting minute pressures from falling droplets and repetitive jumps, enabling real-time monitoring of heartbeat pulses.

In addition to their role in surface microstructures, biomimetic and interlocking structures are widely applied within the internal microstructures as well. Whether it's the spider microcrack structure and lobster exoskeleton structure, or the interlocking fiber-like magnetically induced column forest, they all significantly enhance the sensitivity of sensors.[160] Among these, Zhao and colleagues drew inspiration from the geometric shape of lobster shells.[93] They introduced fragmented Gr sponges and silver nanoparticles into the sensor. Under tensile strain, the stacked Gr inside the sensor underwent mutual sliding rather than direct separation, thereby maintaining the

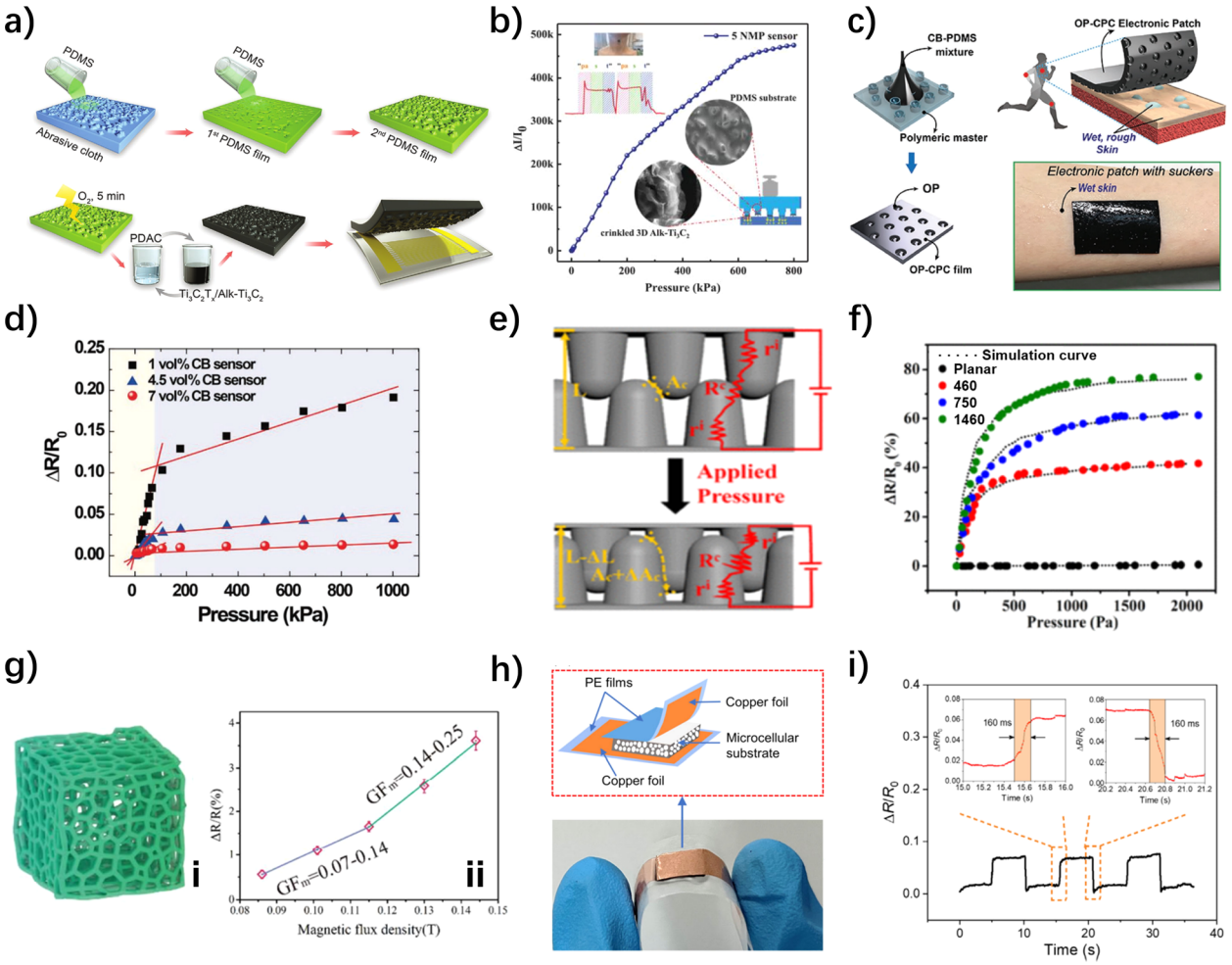

Fig. 6 Different structures for optimizing the sensor performance. (a) The fabrication process of PDMS films syn-thesis and flexible pressure sensors.[154] Reproduced with permission. Copyright at *Advanced Materials Technologies,* 2021 (b) the relative current variations $\Delta I/I_0$ of the sensor under different pressures.[154] Reproduced with permission. Copyright at *Advanced Materials Technologies,* 2021 (c) process steps and application scenarios of OP-CPC electronic placement.[151] Reproduced with permission. Copyright at *Advanced Functional Materials,* 2018 (d) piezoresistive responses of the device subjected to static vertical pressures.[151] Reproduced with permission. Copyright at *Advanced Functional Materials,* 2018 (e) schematic showing resistance composition and the pressure sensing mechanism of the IOCA.[156] Reproduced with permission. Copyright at *ACS Applied Materials & Interfaces,* 2020 (f) experimental resistance changes of the IOCA fitted to theoretically calculated resistance changes.[156] Reproduced with permission. Copyright at *ACS Applied Materials & Interfaces,* 2020 (g) schematic of opening structure: (i) opening structure. (ii) The $\Delta R/R$ *versus* magnetic flux density.[157] Reproduced with permission. Copyright at *ACS Applied Materials & Interfaces,* 2018 (h) schematic of flexible piezoresistive sensor with closed-cell structures structure.[158] Reproduced with permission. Copyright at *Polymer Engineering & Science,* 2023 (i) response and recovery times[158] (1 mm s^{-1} compression speed and 5% strain) reproduced with permission. Copyright at *Polymer Engineering & Science,* 2023.

conductive pathway without breaking, which significantly enlarges the operational range of the sensor.

Likewise, researchers have concentrated on internal porous structures, which provide benefits such as reduced density and lower elastic modulus. Depending on whether their internal voids are open or closed, porous structures can be classified into open-cell and closed-cell structures. Open-cell structures often refer to internal frameworks with high porosity and strong deformability, such as sponge-like structures.[161] Under external forces, the framework of an sponge-like structures.[161] Under external forces, the framework of an open-cell structure begins to undergo compressive deformation, leading to the creation of new contact points between the framework elements, thereby reducing overall resistance. Additionally, the good resilience of sponge-like structures has led many researchers to explore their applications.[162] For instance, sacrificial templates were used by Ding and colleagues to create porous sponge-like flexible tactile sensors capable of detecting pressure, stress, and magnetic fields (Fig. 6g).[157] As the magnetic flux density changes, the GF_m of the sensor changed, ranging from 0.07 to 0.14 and 0.14 to 0.25 in the ranges of 0.086 to 0.115 T and 0.115 to 0.15 T, respectively.

Closed-cell structures, on the other hand, refer to structures with discontinuous bubbles surrounded by solid pore walls, which offer better load-bearing capabilities than open-cell structures. Closed-cell structures provide the sensor with

derived structural elasticity and lower elastic modulus. Furthermore, due to the increase in contact area between the microstructured film caused by bubble deformation and the electrodes under external compression, closed-cell structures can achieve ultra-high sensitivity for low-pressure detection. Pan and colleagues employed PPy to fabricate hollow sphere microstructures through a multiphase reaction, resulting in a flexible resistive tactile sensor capable of detecting pressures below 1 Pa with a response time as low as 50 ms.[111] Li *et al.* achieved tunable piezoresistance and high resilience of the sensor by foaming to form a tunable closed-pore structure in the nanocomposite (Fig. 6h).[158] Owing to the closed-pore structure and the mixed conductive nanofillers (1D MWCNTs and 2D GNPs) distributed in the cell walls, the sensor exhibited shorter response and recovery times, with fast response and recovery within 160 ms after both pressure application and pressure removal (Fig. 6i).

Compared to conventional structures, enhancements have been made in both surface and internal microstructures, enabling the optimal utilization of conductive materials' properties. These structural improvements significantly enhance the performance of flexible resistive tactile sensors, particularly in terms of response and relaxation times and resolution. The performance comparison of flexible resistive tactile sensors with varying structural designs is summarized in Table 3.

3.3.2. Sensor integration and arrays. Individual units of flexible resistive tactile sensors typically capture signals that are notably weak and prone to instability. Therefore, it becomes necessary to introduce amplification and filtering circuits to enhance and stabilize these signals, guaranteeing consistent and dependable monitoring data.[163] Furthermore, for the purpose of multi-point monitoring and the perception of three-dimensional forces, it is common practice to integrate these units into array structures. This integration involves the utilization of multiple units to produce distinct responses to physical stimuli, thereby allowing the reconstruction of three-dimensional force magnitudes and directions or the spatial distribution of external factors like temperature, humidity, and magnetic field intensity.[164]

Common array structures frequently adopt the checkerboard pattern, comprising an $x \times y$ array of flexible resistive tactile sensor units, offering a straightforward and dependable approach to monitoring. Researchers have used this checkerboard structure to detect the magnitude and distribution of gravitational forces acting on objects. Zhao and colleagues utilized laser direct writing (LDW) technology to create a high-performing, flexible asymmetric pressure sensor from multi-walled carbon nanotubes (MWCNTs) and laser-induced graphene (LIG). This sensor boasted an integrated sensing array with multi-point recognition, enabling the detection of objects with varying loads (Fig. 7a).[165] Furthermore, magneto-sensitive flexible tactile sensor units have been employed by scholars to construct checkerboard arrays that can detect non-contact gesture actions through force sensing, enhancing their applicability in human–machine interaction.[160]

Multi-unit monitoring in an array structure can also be used to perceive the magnitude and direction of three-dimensional forces. Typically, the pressures experienced by each stimulated sensor unit follow a pattern from small to large in the direction of force application, and analyzing the distinct response signals from each unit to directional forces enables data decoupling into magnitude and direction.[166] However, this structure might not provide very precise resolution for the direction of three-dimensional forces (for example, the response difference between forces at 30° and 60° directions is not significant). Common solutions include increasing the number of sensor units, reducing the sensor unit's area, and optimizing the decoupling algorithm. Furthermore, Zhao and colleagues were inspired by fish fins to create a fin-like double-sided array of flexible electronic skin (Fig. 7b).[166] The fin-like double-sided array structure offered more accurate perception of force direction because when one side of this electronic skin experienced external force, the other side responded synchronously.

3.3.3. Sensor calibration and decoupling. In practical applications of resistive touch sensors, deducing the mathematical relationship between input three-dimensional forces, sensor deformations, and changes in sensor output response through theoretical mathematical derivation is challenging, especially when dealing with flexible resistive touch sensor arrays used in electronic skin. Establishing the relationship between external input stimuli and the responses of individual units, which is crucial for monitoring signals like three-dimensional forces, ambient temperature, humidity, object proximity, *etc.*, is challenging and often necessitates a significant amount of experimental data. Amidst a range of

Table 3 Performance comparison of the sensors with different structural designs

Type	Structural designs	Response and relaxation time	Resolution	Reference
Surface microstructures	Curved folds structures	10 ms, 20 ms	1 Pa	147
	Biomimetic structures	1 ms, 0.5 ms	0.1 Pa	155
	Interlocking structures	48 ms, 56 ms	0.98 Pa	156
	Cone-like structures	24 ms, 36 ms	16 Pa	148
	Hemispherical structures	35 ms, 50 ms	0.4 Pa	149
Internal porous structures	Biomimetic structures	20 ms, 20 ms	—	93
	Interlocking structures	20 ms, 20 ms	—	93
	Open-cell structures	200 ms, 200 ms	4.1 Pa	161
	Closed-cell structures	160 ms, 160 ms	0.8 kPa	158

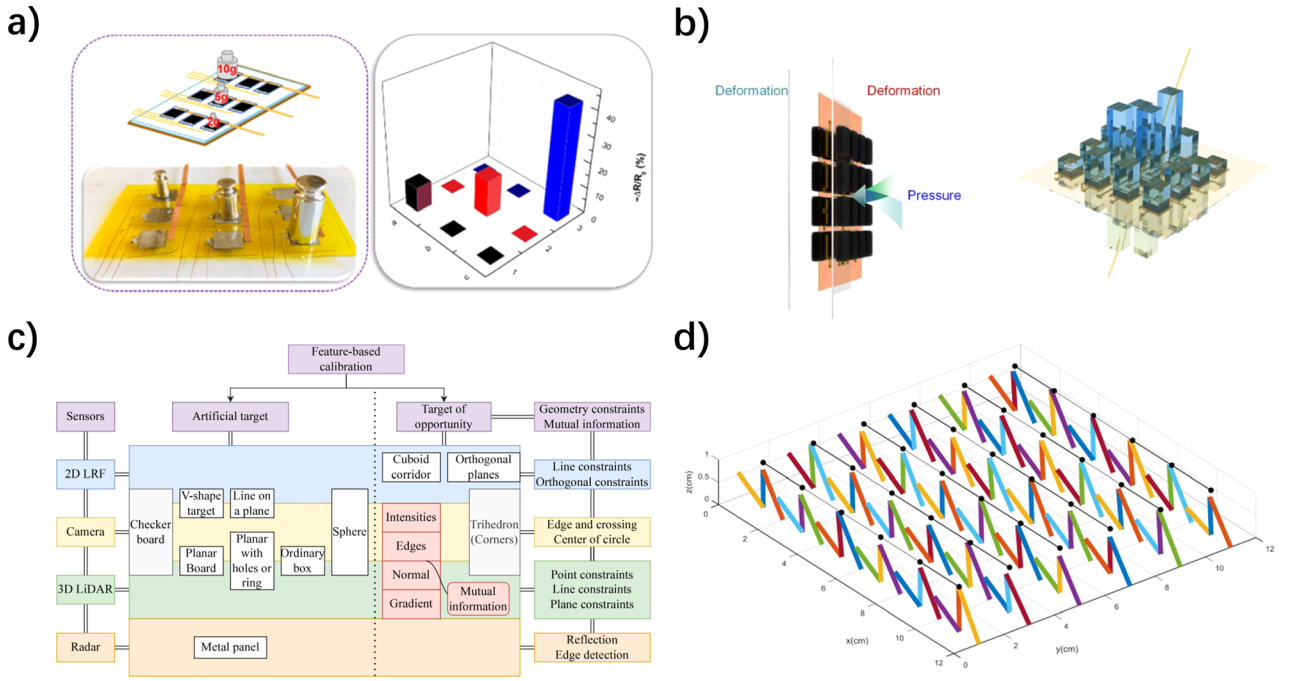

Fig. 7 Integration, arrays, optimized calibration and decoupling algorithms are all important ways to ensure the stability of the information acquired and transmitted by the sensor. (a) Optical image and the relative resistance response mapping of pressure of a 3 × 3 pixel sensory array positioned different loads (2, 5 and 10 g).[165] Reproduced with permission. Copyright at *Sensors and Actuators A: Physical*, 2021 (b) the schematic diagram of the fin-like double-side CNTs sponge-based sensor array subjects to external force changes and identifies force direction.[166] Reproduced with permission. Copyright at *ACS Applied Materials & Interfaces*, 2020 (c) different feature-based calibration methods for different sensors according to their individual constraints.[167] Reproduced with permission. Copyright at *Information Fusion*, 2023 (d) the deformation of the sensitive units when the force components are applied on it.[168] Reproduced with permission. Copyright at *Micromachines*, 2018.

decoupling techniques, it becomes vital to integrate sensor structures with empirical data for calibrating input–output relationships and constructing mathematical models, especially when striving for optimal algorithms.

Calibration, in the context of flexible resistive touch sensors, involves employing standard equipment to ascertain the sensor's input–output relationship. Due to variations between theoretical ideals and real-world characteristics, often stemming from the choice of flexible substrate and conductive materials, calibration experiments are essential for identifying and addressing these discrepancies. Through calibration experiments, discrepancies can be pinpointed, their origins analyzed, and the sensor's structure and model can be refined and enhanced accordingly (Fig. 7c).[167] Currently, calibration methods often involve using weights for loading.

Decoupling methods entail using algorithms to correct the input–output relationship of a multivariable system, reducing or eliminating interdependencies to convert the system into multiple single-input single-output systems.[169] Presently, decoupling techniques can be broadly classified into three categories: methods utilizing the least squares approach, those employing fuzzy reasoning, and those relying on neural networks.[170] H However, these decoupling techniques come with their respective limitations. For instance, the least squares method is constrained by linear estimation. Fuzzy reasoning can be subjective when determining weight vectors for indicators, particularly with large sets of indicators, potentially resulting in reduced resolution. Neural networks, while proficient in swiftly finding optimal solutions thanks to their self-learning ability, can be critiqued for their lack of transparent reasoning processes and explanations, as they heavily rely on data for learning. Among these methods, neural networks excel due to their self-learning capabilities and high-speed optimization, which result in improved decoupling accuracy. For instance, Song *et al.* employed a backpropagation (BP) neural network to successfully decouple three-dimensional forces on a 6 × 6 flexible array touch sensor.[168] The sensor consists of numerous sensitive units, each with two upper tactile sensing electrodes at its top. When force components along the *X* and *Z* directions are applied to the sensor, the tactile sensor array undergoes deformation. If the original position of one of the two upper tactile sensing electrodes is represented by a black dot, Fig. 7d illustrates a deformation state of the sensor. According to the established mathematical model of the sensor, coupled with the backpropagation (BP) neural algorithm, the force state applied to the sensor can be accurately inferred. Consequently, the decoupling accuracy of force sensing is effectively enhanced.

3.4. Optimization and applications in extreme scenarios

The lifespan of flexible resistive tactile sensors is influenced by various factors, including material durability, design quality, working environment, frequency of use, maintenance, and upkeep. Among these factors, the working environment is

a crucial element that cannot be overlooked. In extreme environments, the durability and reliability of conventional flexible resistive tactile sensors significantly decrease, leading to impaired signal output. Besides mechanical extreme conditions such as excessive stretching, compression, and bending, environmental factors like cold temperatures, high heat, polluted conditions, and varying humidity also profoundly impact sensor performance. An excellent flexible resistive tactile sensor must undergo targeted optimizations to ensure proper functionality in such extreme conditions.

3.4.1. Extreme temperatures. Certain elastomers and conductive materials may become brittle at low temperatures and lose elasticity at high temperatures. To ensure the reliability of flexible resistive tactile sensors, materials maintaining elasticity and stability at extreme temperatures can be chosen. Additionally, incorporating insulation layers in the design can help prevent electrical issues in extreme temperature conditions. Zhao *et al.* have developed an aerogel using a PEDOT:PSS aqueous solution and PI precursor, which maintains structural stability in environments ranging from as low as −15 degrees to as high as 120 degrees Celsius.[118] Wang *et al.* have developed a novel electrospun nanofiber-reinforced three-dimensional (3D) reduced graphene oxide aerogel (GA) using polyacrylonitrile (PAN) and polystyrene sulfonate (PSAN). In the case of GA-1, compressing at the same strain under −60 °C, the maximum strength does not show a significant decrease with prolonged insulation time.[171] The synergistic effect of sulfonyl groups and benzene ring double bonds in PSAN nanofibers allows the sensor to maintain nearly constant maximum compressive strength during a 12 hour insulation test at 200 °C. The retention rates of diameter, height, and mass are all above 95%. These findings clearly indicate that material and structural innovations are crucial for improving the temperature resistance of sensors.

3.4.2. Contaminated environments. In contaminated environments, dust, liquids, or other pollutants may enter the interior of the sensor, affecting its performance. Therefore, the design of sensors in such environments may consider adopting a sealed structure or using hydrophobic surface coatings to reduce sensitivity to contamination. Huang *et al.* developed a superelastic graphene aerogel using freeze-casting technology and natural drying techniques.[172] This graphene aerogel exhibits excellent mechanical properties, high conductivity, and oil–water separation capabilities, making it a promising candidate for applications in flexible sensors and the cleanup of organic pollution or oil spills. Altynay Kaidarova *et al.* utilized the piezoresistive effect of three-dimensional porous graphene, using laser printing of graphene on polyimide film to develop a flexible pressure sensor.[173] The application of a polymethyl methacrylate coating proves highly advantageous in underwater scenarios. This coating serves to shield the sensors from biofouling and shunt currents, allowing them to function effectively at depths of up to 2 kilometers in the highly saline waters of the Red Sea.

3.4.3. Different humidity conditions. In high humidity environments, adopting a waterproof design for the sensor, including the use of waterproof materials and sealing techniques, is essential to ensure its stability and reliability. Additionally, in sensor design, consideration should be given to the impact of humidity on resistance. Humidity compensation techniques can be introduced to enhance measurement accuracy. Tian *et al.* developed an all-fabric pressure-sensitive sensor (AFPS) by adding hydrophobic perfluorodecyltrichlorosilane (FTS), hindering condensation in the conductive network. The sensor demonstrated excellent anti-fouling and humidity resistance properties.[174] In a closed environment with 90% relative humidity (RH), the sensor's electrical conductivity can be well-maintained. Zhao *et al.* developed a flexible lateral resistive sensor with a mechanical transduction structure, employing a semi-encapsulated design.[175] The sensing layer (three-dimensional nanowire network) is encapsulated within the fabricated sensor body and protected by PDMS, demonstrating excellent humidity stability.

4. Applications of flexible resistive tactile sensor

With increasing demands for intelligent machinery and complex working environments, the role of sensors in acquiring extensive information becomes crucial. Flexible resistive tactile sensors, renowned for their sensitivity, biocompatibility, and flexibility, excel in applications where rigid sensors fall short. Their robust tensile properties and ductility make them suitable for large-scale deformation data monitoring, while their precision and flexibility are advantageous in medical testing. Additionally, their stress perception and self-healing capabilities find applications in robotic contact sensing, leading to diverse and convenient applications that enhance our daily lives.

4.1. Tactile perception and human–machine interaction

Human touch sensors grant us the ability to perceive numerous object characteristics, including shape, size, texture, and more, enabling sensory cognition and informed actions.[176] Just as essential as they are to humans, imparting machines with tactile perception capabilities is a primary research goal to enhance their capabilities in industries like manufacturing, healthcare, and services.[177]

With the emergence and application of various flexible resistive tactile sensors, flexible devices have replaced some rigid sensors, leading to improved safety and deformation resistance of machines.[178] For instance, flexible tactile sensors simulated from human fingerprints, as developed by Wang *et al.*, could detect various stresses such as compression, stretching, vibrations, and sliding (Fig. 8a).[179] The strain signal of this sensor was highly synchronized with the applied pressure, which contributed to the real-time perception of the machine (Fig. 8b). In addition to tactile perception, flexible resistive tactile sensors hold significant potential in the field of human–machine interaction. By integrating flexible resistive tactile sensors into smart gloves or electronic skins, thanks to mature control systems, advantages in information acquisition, from gravity analysis to gesture recognition and motion monitoring, can be fully exploited. Amjadi *et al.*, for example, utilized

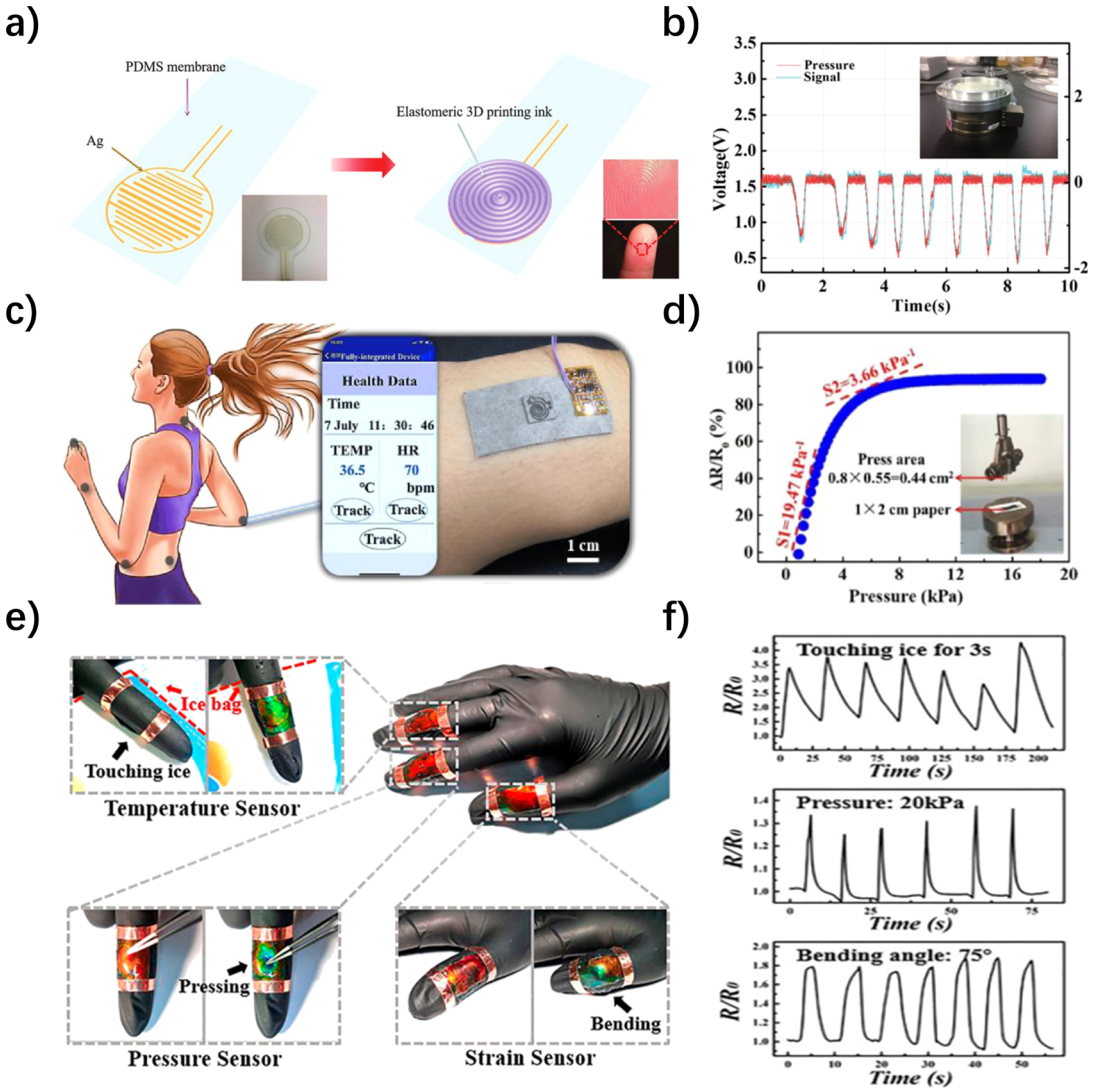

Fig. 8 The application of flexible resistive tactile pressure sensors for tactile sensing, human–computer interaction, healthcare and e-skin. (a) Schematic diagram of the preparation process of pressure-sensing.[179] Reproduced with permission. Copyright at *Advanced Materials Technologies*, 2019 (b) output signal and pressure as the function of time.[179] Reproduced with permission. Copyright at *Advanced Materials Technologies*, 2019 (c) the fully-integrated wearable electronic device attached to the skin and signals acquisition with a cellphone.[182] Reproduced with permission. Copyright at *Sensors and Actuators A: Physical*, 2021 (d) resistance changes *versus* different pressures.[182] Reproduced with permission. Copyright at *Sensors and Actuators A: Physical*, 2021 (e) schematics and the optical images of the E-skins attached to human fingers. Three red-colored E-skins are affixed on different fingers and detect temperature, pressure, and tension, respectively.[183] Reproduced with permission. Copyright at *Proceedings of the National academy of Sciences of the United States of America*, 2020 (f) the real-time signals of the variation of resistance of the E-skin under different test conditions.[183] Reproduced with permission. Copyright at *Proceedings of the National academy of Sciences of the United States of America*, 2020.

Ag NW-based flexible strain sensors to create a smart glove system for monitoring finger bending and various hand gestures.[87] This smart glove integrated a chip combining data collection and wireless communication systems to acquire sensor data and perform corrections. Furthermore, Yuan *et al.*'s electronic skin model could monitor the location of applied force as well as movements of the knee joint, such as walking, jumping, and squatting.[145]

4.2. Medical and health monitoring

The growing societal demands have led to an increased prevalence of cardiovascular diseases, posing health risks to a larger population. In today's fast-paced lives, individuals are placing greater emphasis on monitoring physiological parameters like heart rate, pulse, and blood pressure.[180] As a result, smart wristbands for heart rate monitoring have gained popularity. Yet, traditional methods like power-hungry photoplethysmography and complex ECG signal testing fall short of meeting people's needs. Hence, researchers are turning their attention to the vibration measurement method employing flexible resistive tactile sensors.[181]

The vibration measurement method captures the body's vibration signals caused by each heartbeat using high-precision flexible tactile sensors and obtains the heart rate through signal

processing. A highly sensitive pressure sensor developed by Liu's research team could detect three peaks of the arterial pulse wave (anacrotic wave, tidal wave, and dicrotic wave).[110] Furthermore, Zhang and colleagues have created a washable, breathable, and flexible tactile sensor, capable of monitoring breathing, pulse, and temperature (Fig. 8c).[182] This sensor exhibited high sensitivity, registering at 19.47 kPa^{-1} within the small pressure range of 0–4 kPa, and 3.66 kPa^{-1} within the larger pressure range of 4–20 kPa (Fig. 8d). The data collected by this sensor could be conveniently and efficiently transmitted to mobile devices *via* Bluetooth for further analysis and ease of access.

Apart from heart rate monitoring, to address the challenge of environment perception for people with disabilities, some researchers are exploring how to directly convey collected signals to biological neural networks. Kim *et al.*, for example, have worn their developed smart prosthetic skin capable of monitoring stress, temperature, and humidity on a prosthetic limb.[153] They connected the signals collected by this electronic skin to multiple electrodes connected to the sciatic nerve of rats' hind legs, successfully transmitting the signals to the rats' central nervous system.

4.3. Electronic skins

With the rise of the field of artificial intelligence in recent years, multifunctional electronic skins for both humans and robots have become a focus of attention.[184,185] E-skin, utilizing state-of-the-art flexible piezoresistive haptic sensors, closely emulates real skin in its sensing approach, providing a comprehensive record of environmental and object data through its exceptional flexibility and snug fit in contact sensing. Zhang *et al.* proposed an e-skin based on a composite liquid crystal hydrogel of hydroxypropyl cellulose (HPC), polyacrylamide-acrylic acid (PACA) and CNTs (Fig. 8e).[183] The addition of HPC and PACA gave the e-skin the ability to feedback the stimulation site, and the addition of CNTs made the ability even more powerful, allowing it to provide quantitative feedback on environmental data such as temperature, pressure, bending angle, *etc.* (Fig. 8f). Zou *et al.* also doped conductive silver nanoparticles in a dynamic covalent thermosetting material to develop a repairable, recyclable and malleable electronic skin.[186] In addition to its basic function of sensing environmental forces, the skin achieved advanced functionalities including full recyclability and multiple sensing of temperature, humidity, and flow. Likewise, Jo *et al.* explored multifunctional flexible resistive tactile sensors and converted them into electronic skins, granting robots human-like tactile sensing capabilities as well as functions like electromagnetic shielding and heat insulation.[187]

Although these applications are conceptual, some companies have already introduced commercial products of flexible resistive tactile sensors in practice. Companies such as Tekscan and Pressure Profile Systems are notable examples. They specialize in providing flexible tactile sensor solutions for measuring and analyzing pressure distribution, widely applied in the fields of healthcare, industry, human–machine interaction, and research. These products, by real-time and accurate measurement of pressure distribution, have the potential to enhance medical treatments, improve industrial production efficiency, and bring more convenience and innovation to society.

5. Conclusions and perspectives

Flexible resistive tactile sensors, in recent decades, have made significant strides and hold promise for electronic skin applications. High-flexibility materials like PDMS, PET, PU, and Ecoflex as substrates, paired with excellent conductive materials such as AgNW, Gr, CNTs, PPy, MXene, and conducting polymers as sensing elements were employed, resulting in sensors with remarkable properties including stretchability, sensitivity, and linearity. Furthermore, sensors featuring microstructures, particularly those with interlocking and porous designs, exhibit heightened sensitivity, enabling the detection of subtle stresses within an extremely low range. Nonetheless, the integration of these sensors into electronic skin poses challenges, necessitating further research and development.

Firstly, a balance between high flexibility and high sensitivity is still challenging to achieve in flexible resistive tactile sensors. While some sensors have achieved high sensitivity within a low operating range, extending this performance to a broader operating range remains limited. Secondly, flexible resistive tactile sensors are difficult to tailor and join, and large-area coverage remains challenging. Although the performance of individual sensing units has improved, their scalability is poor, and they cannot be easily tailored or joined to different carrier conditions. Furthermore, the fabrication process of electronic skin is complex, and the high cost of production hampers its scalability. Additionally, the large-scale array of sensing units and complex signal readout circuits with limited sampling rates can hinder real-time data acquisition. Finally, the high power consumption of electronic skin and shortcomings in intelligent algorithms are also limiting factors. High power consumption in the circuits requires significant electrical energy, and the high-density tactile image demands specialized intelligent algorithms for intelligent recognition and perception of tactile objects.

However, the existing limitations of electrically flexible resistive tactile sensors also indicate the future directions for improvement. With the rapid development of intelligent robots and the widespread adoption of mobile smart devices, flexible resistive tactile sensors are showing great potential for applications in machine tactile sensing systems and flexible human–machine interaction networks. Additionally, tactile sensing systems can enhance a robot's self-learning and adaptability, allowing them to operate not only in safe workspaces but also in extreme and harsh environments, making greater contributions in manufacturing, services, healthcare, and defence industries. Moreover, integrated electronic skin with flexible resistive tactile sensors can develop towards multi-functionality, anti-interference, self-healing, and self-cleaning, achieving a comprehensive tactile perception performance more akin to human skin. This will enable robots to better adapt to complex

external environments. Electronic skin will hold substantial practical value in fields such as biomimetic robotics, healthcare, and more.

Currently, flexible resistive tactile sensors not only need to mimic the comprehensive sensing abilities of human skin, such as pressure, stress, temperature, humidity, proximity, and surface roughness, but also need to evolve towards flexibility, lightweight, transparency, integration, multi-functionality, low power consumption, self-healing, self-cleaning, and high resolution. However, due to issues such as the trade-off between high flexibility and high sensitivity, poor compatibility, limited scalability, difficulties in large-scale coverage, complex manufacturing processes, high costs, and high energy consumption, the widespread implementation of flexible resistive tactile sensors in human society remains challenging.

In the future, the most critical research for flexible resistive tactile sensors should focus on achieving a balance between high flexibility, wide operating range, high sensitivity, multifunctionality, self-healing, self-cleaning, interference resistance, and transparency. This will enable them to make significant contributions to protecting against external interferences, monitoring human health, perceiving posture and motion, assisting in mechanical operations, and sensing the external environment for the benefit of human society. In the future, electrically flexible resistive tactile sensors will continue to face new challenges, such as transparency, biocompatibility, biodegradability, neural interface control, high integration, and miniaturization. Developing high-performance, easily manufacturable, and scalable electrically flexible resistive tactile sensors for widespread integration across various domains of human society is the direction of its future development.

Conflicts of interest

The authors declare that they have no known competing financial interests or personal relationships that could have appeared to influence the work reported in this paper.

Acknowledgements

This work was financially supported by the Natural Science Research Start-up Foundation of Recruiting Talents of Nanjing University of Posts and Telecommunications (Grant No. NY221111, NY221003), Natural Science Foundation of the Higher Education Institutions of Jiangsu Province (Grant No. 22KJB430038), and Natural Science Foundation of Jiangsu Province of China (BK20230359) and National Natural Science Foundation of China (62304112) awarded to Yang Li. Zhiwei Liu thanks the support from the National Natural Science Foundation Program of China (No. 52204370).

Notes and references

1 S. Yuan, C. Ma, E. Fetaya, T. Mueller, D. Naveh, F. Zhang and F. Xia, *Science*, 2023, **379**, eade1220.
2 J. T. Atkinson, L. Su, X. Zhang, G. N. Bennett, J. J. Silberg and C. M. Ajo-Franklin, *Nature*, 2022, **611**, 548–553.
3 H. C. Ates, P. Q. Nguyen, L. Gonzalez-Macia, E. Morales-Narváez, F. Güder, J. J. Collins and C. Dincer, *Nat. Rev. Mater.*, 2022, **7**, 887–907.
4 Y. Li, B. Cui, S. Zhang, B. Li, J. Li, S. Liu and Q. Zhao, *Small*, 2022, **18**, 2107413.
5 J.-C. Hsieh, Y. Li, H. Wang, M. Perz, Q. Tang, K. W. K. Tang, I. Pyatnitskiy, R. Reyes, H. Ding and H. Wang, *J. Mater. Chem. B*, 2022, **10**, 7260–7280.
6 X. Li, Q. Xu, Y. Tang, C. Hu, J. Niu and C. Xu, *IEEE Sens. J.*, 2023, **23**, 14773–14780.
7 H. Ikeuchi and H. Saito, *IEEE Sens. J.*, 2022, **22**, 10740–10750.
8 M. Chen, D. Cui, Z. Zhao, D. Kang, Z. Li, S. Albawardi, S. Alsageer, F. Alamri, A. Alhazmi, M. R. Amer and C. Zhou, *Nano Res.*, 2022, **15**, 5510–5516.
9 J.-C. Hsieh, H. Alawieh, Y. Li, F. Iwane, L. Zhao, R. Anderson, S. I. Abdullah, K. W. Kevin Tang, W. Wang, I. Pyatnitskiy, Y. Jia, J. d. R. Millán and H. Wang, *Biosens. Bioelectron.*, 2022, **218**, 114756.
10 S. Zhang, Y. Li, G. Tomasello, M. Anthonisen, X. Li, M. Mazzeo, A. Genco, P. Grutter and F. Cicoira, *Adv. Electron. Mater.*, 2019, **5**, 1900191.
11 Y. Li, S. Zhang, X. Li, V. R. N. Unnava and F. Cicoira, *Flexible Printed Electron.*, 2019, **4**, 044004.
12 S. Pyo, J. Lee, K. Bae, S. Sim and J. Kim, *Adv. Mater.*, 2021, **33**, 2005902.
13 S. Sim, E. Jo, Y. Kang, E. Chung and J. Kim, *Small*, 2021, **17**, 2105334.
14 B. Ji, Q. Zhou, M. Lei, S. Ding, Q. Song, Y. Gao, S. Li, Y. Xu, Y. Zhou and B. Zhou, *Small*, 2021, **17**, 2103312.
15 S. Hamaguchi, T. Kawasetsu, T. Horii, H. Ishihara, R. Niiyama, K. Hosoda and M. Asada, *IEEE Robot. Autom. Lett.*, 2020, **5**, 4028–4034.
16 F. Qi, L. Xu, Y. He, H. Yan and H. Liu, *Cryst. Res. Technol.*, 2023, **58**, 2300119.
17 X. Qu, J. Xue, Y. Liu, W. Rao, Z. Liu and Z. Li, *Nano Energy*, 2022, **98**, 107324.
18 G. Canavese, S. Stassi, C. Fallauto, S. Corbellini, V. Cauda, V. Camarchia, M. Pirola and C. F. Pirri, *Sens. Actuators, A*, 2014, **208**, 1–9.
19 A. P. Gerratt, H. O. Michaud and S. P. Lacour, *Adv. Funct. Mater.*, 2015, **25**, 2287–2295.
20 Y. Gao, H. Ota, E. W. Schaler, K. Chen, A. Zhao, W. Gao, H. M. Fahad, Y. Leng, A. Zheng, F. Xiong, C. Zhang, L.-C. Tai, P. Zhao, R. S. Fearing and A. Javey, *Adv. Mater.*, 2017, **29**, 1701985.
21 C. Wu, T. W. Kim, J. H. Park, B. Koo, S. Sung, J. Shao, C. Zhang and Z. L. Wang, *ACS Nano*, 2020, **14**, 1390–1398.
22 J. Wang, P. Cui, J. Zhang, Y. Ge, X. Liu, N. Xuan, G. Gu, G. Cheng and Z. Du, *Nano Energy*, 2021, **89**, 106320.
23 D. Lu, T. Liu, X. Meng, B. Luo, J. Yuan, Y. Liu, S. Zhang, C. Cai, C. Gao, J. Wang, S. Wang and S. Nie, *Adv. Mater.*, 2023, **35**, e2209117.
24 Y. Lu, D. Kong, G. Yang, R. Wang, G. Pang, H. Luo, H. Yang and K. Xu, *Adv. Sci.*, 2023, 2303949.
25 L. Chen, Y. Xu, Y. Liu, J. Wang, J. Chen, X. Chang and Y. Zhu, *ACS Appl. Mater. Interfaces*, 2023, **15**, 24923–24932.

26 H. Hu, C. Zhang, C. Pan, H. Dai, H. Sun, Y. Pan, X. Lai, C. Lyu, D. Tang, J. Fu and P. Zhao, *ACS Nano*, 2022, **16**, 19271–19280.
27 M. Yang, Y. Cheng, Y. Yue, Y. Chen, H. Gao, L. Li, B. Cai, W. Liu, Z. Wang, H. Guo, N. Liu and Y. Gao, *Adv. Sci.*, 2022, **9**, 2200507.
28 D. Yu, Z. Zheng, J. Liu, H. Xiao, G. Huangfu and Y. Guo, *Nano-Micro Lett.*, 2021, **13**, 117.
29 R. Yu, T. Xia, B. Wu, J. Yuan, L. Ma, G. J. Cheng and F. Liu, *ACS Appl. Mater. Interfaces*, 2020, **12**, 35291–35299.
30 W. Du, Z. Li, Y. Zhao, X. Zhang, L. Pang, W. Wang, T. Jiang, A. Yu and J. Zhai, *Chem. Eng. J.*, 2022, **446**, 137268.
31 J. Tolvanen, J. Hannu and H. Jantunen, *IEEE Sens. J.*, 2017, **17**, 4735–4746.
32 Y. Zou, J. Liao, H. Ouyang, D. Jiang, C. Zhao, Z. Li, X. Qu, Z. Liu, Y. Fan, B. Shi, L. Zheng and Z. Li, *Appl. Mater. Today*, 2020, **20**, 100699.
33 L. Huang, S. Wang, P. Zhang, K. Zhang, Y. Li and Z. Chen, *Adv. Mater. Technol.*, 2024, **9**, 2301377.
34 M. Kong, Z. Xiang, X. Xu, S. Ma, C. Chen, X. Wang, K. Li and D. Wei, *Adv. Electron. Mater.*, 2023, **9**, 2300197.
35 D. Guo, P. Guo, Y. Yao, L. Ren, M. Jia, W. Wang, Y. Wang, Y. Zhang, A. Yu and J. Zhai, *Nano Energy*, 2022, **100**, 107508.
36 H. R. Na, H. J. Lee, J. H. Jeon, H.-J. Kim, S.-K. Jerng, S. B. Roy, S.-H. Chun, S. Lee and Y. J. Yun, *npj Flexible Electron.*, 2022, **6**, 2.
37 J. Cai, Y. He, Y. Zhou, H. Yu, B. Luo and M. Liu, *Composites, Part A*, 2022, **155**, 106813.
38 R. Chen, Z. He, X. Luo, M. Wang, Z. Liu, Y. Wu, X. Dong, D. Zhang and J. Liu, *ACS Appl. Polym. Mater.*, 2022, **5**, 391–399.
39 W. B. Han, G. J. Ko, K. G. Lee, D. Kim, J. H. Lee, S. M. Yang, D. J. Kim, J. W. Shin, T. M. Jang, S. Han, H. Zhou, H. Kang, J. H. Lim, K. Rajaram, H. Cheng, Y. D. Park, S. H. Kim and S. W. Hwang, *Nat. Commun.*, 2023, **14**, 2263.
40 L. Zhang, T. Song, L. Shi, N. Wen, Z. Wu, C. Sun, D. Jiang and Z. Guo, *J. Nanostruct. Chem.*, 2021, **11**, 323–341.
41 J. Miao and T. Fan, *Carbon*, 2023, **202**, 495–527.
42 S. He, Y. Hong, M. Liao, Y. Li, L. Qiu and H. Peng, *Aggregate*, 2021, **2**, e143.
43 B. C. Zhang, Y. H. Shi, J. Mao, S. Y. Huang, Z. B. Shao, C. J. Zheng, J. S. Jie and X. H. Zhang, *Adv. Mater.*, 2021, **33**, e2008171.
44 Y. Zhang, Q. Lu, J. He, Z. Huo, R. Zhou, X. Han, M. Jia, C. Pan, Z. L. Wang and J. Zhai, *Nat. Commun.*, 2023, **14**, 1252.
45 Y. Li, J. Long, Y. Chen, Y. Huang and N. Zhao, *Adv. Mater.*, 2022, **34**, e2200517.
46 Y. Yan, Z. Hu, Z. Yang, W. Yuan, C. Song, J. Pan and Y. Shen, *Sci. Robot.*, 2021, **6**, eabc8801.
47 Y.-R. Ding, C.-H. Xue, Q.-Q. Fan, L.-L. Zhao, Q.-Q. Tian, X.-J. Guo, J. Zhang, S.-T. Jia and Q.-F. An, *Chem. Eng. J.*, 2021, **404**, 126489.
48 L. Wang, F. Xia, W. Xu, G. Wang, S. Hong, F. Cheng, B. Wu and N. Zheng, *Adv. Funct. Mater.*, 2023, **33**, 2215127.
49 K. Liu, C. Yang, S. Zhang, Y. Wang, R. Zou, Alamusi, Q. Deng and N. Hu, *Mater. Des.*, 2022, **218**, 110689.
50 A. Rivadeneyra, A. Marín-Sánchez, B. Wicklein, J. F. Salmerón, E. Castillo, M. Bobinger and A. Salinas-Castillo, *Compos. Sci. Technol.*, 2021, **208**, 108738.
51 M. Korrapati, S. Chauhan, Y. Tang and D. Gupta, *Macromol. Mater. Eng.*, 2022, **307**, 2200132.
52 X. Li, J. Liu, Q. Guo, X. Zhang and M. Tian, *Small*, 2022, **18**, e2201012.
53 K.-X. Hou, S.-P. Zhao, D.-P. Wang, P.-C. Zhao, C.-H. Li and J.-L. Zuo, *Adv. Funct. Mater.*, 2021, **31**, 2107006.
54 H. S. Cho, H. Y. Moon, H. S. Lee, Y. T. Kim and S. C. Jeoung, *Bull. Korean Chem. Soc.*, 2021, **42**, 1225–1231.
55 J. Vaicekauskaite, P. Mazurek, S. Vudayagiri and A. L. Skov, *J. Mater. Chem. C*, 2020, **8**, 1273–1279.
56 K. Anasiewicz and J. Kuczmaszewski, *Materials*, 2022, **15**, 8060.
57 Y. Tai, T. Chen and G. Lubineau, *ACS Appl. Mater. Interfaces*, 2017, **9**, 32184–32191.
58 S. Wang, K. Chen, M. Wang, H. Li, G. Chen, J. Liu, L. Xu, Y. Jian, C. Meng, X. Zheng, S. Liu, C. Yin, Z. Wang, P. Du, S. Qu and C. W. Leung, *J. Mater. Chem. C*, 2018, **6**, 4737–4745.
59 Z.-X. Li, X.-Y. Gao, P. Huang, Y.-Q. Li and S.-Y. Fu, *J. Mater. Chem. A*, 2022, **10**, 9114–9120.
60 Q. Lin, F. Zhang, X. Xu, H. Yang, Q. Mao, D. Xian, K. Yao and Q. Meng, *Nanomaterials*, 2023, **13**, 2630.
61 A. Mokhtari, N. Tala-Ighil and Y. A. Masmoudi, *J. Mater. Eng. Perform.*, 2021, **31**, 2715–2722.
62 X. Hong, L. Zou, J. Zhao, C. Li and L. Cong, *IOP Conf. Ser.: Mater. Sci. Eng.*, 2018, **439**, 042011.
63 Y. Lou, H. Liu and J. Zhang, *Chem. Eng. J.*, 2020, **399**, 125732.
64 T.-L. Chu, C. Ha-Minh and A. Imad, *Composites, Part B*, 2016, **95**, 144–154.
65 F. Xu, W. Fan, Y. Zhang, Y. Gao, Z. Jia, Y. Qiu and D. Hui, *Composites, Part B*, 2017, **116**, 398–405.
66 S. Fu, B. Yu, W. Tang, M. Fan, F. Chen and Q. Fu, *Compos. Sci. Technol.*, 2018, **163**, 141–150.
67 M. S. H. Al-Furjan, L. Shan, X. Shen, M. S. Zarei, M. H. Hajmohammad and R. Kolahchi, *J. Mater. Res. Technol.*, 2022, **19**, 2930–2959.
68 S. Wang, S. Xuan, M. Liu, L. Bai, S. Zhang, M. Sang, W. Jiang and X. Gong, *Soft Matter*, 2017, **13**, 2483–2491.
69 D. Yang, H. K. Nam, T.-S. D. Le, J. Yeo, Y. Lee, Y.-R. Kim, S.-W. Kim, H.-J. Choi, H. C. Shim, S. Ryu, S. Kwon and Y.-J. Kim, *ACS Nano*, 2023, **17**, 18893–18904.
70 G. Tian, L. Zhan, J. Deng, H. Liu, J. Li, J. Ma, X. Jin, Q. Ke and C. Huang, *Chem. Eng. J.*, 2021, **425**, 130682.
71 K. Liu, J. Yu, Y. Li, X. Yan, D. Bai, X. Liao, Z. Zhou, Y. Gao, X. Yang and L. Li, *Adv. Mater. Technol.*, 2019, **4**, 1900475.
72 P. M. Pataniya, C. K. Sumesh, M. Tannarana, C. K. Zankat, G. K. Solanki, K. D. Patel and V. M. Pathak, *Nanotechnology*, 2020, **31**, 435503.
73 J. Huang, Y. Cai, C. Xue, J. Ge, H. Zhao and S.-H. Yu, *Nano Res.*, 2021, **14**, 3636–3642.
74 X. Dai, P. Li, Y. Sui and C. Zhang, *J. Polym. Sci.*, 2021, **59**, 627–637.

75 A. Dallinger, K. Keller, H. Fitzek and F. Greco, *ACS Appl. Mater. Interfaces*, 2020, **12**, 19855–19865.
76 T.-P. Huynh and H. Haick, *Adv. Mater.*, 2016, **28**, 138–143.
77 M. Zhang, X. Xia, L. Zhang, G. Zhao, C. Liu, N. Li, J. Xu, Y. Chen and X. Jian, *Eur. Polym. J.*, 2023, **191**, 112018.
78 G. Dias, M. Prado, R. Ligabue, M. Poirier, C. Le Roux, P. Micoud, F. Martin and S. Einloft, *Polym. Polym. Compos.*, 2018, **26**, 127–140.
79 Y. Luo, L. Zhao, G. Luo, L. Dong, Y. Xia, M. Li, Z. Li, K. Wang, R. Maeda and Z. Jiang, *Microsyst. Nanoeng.*, 2023, **9**, 113.
80 T. Yao, S. Han, C. Men, J. Zhang, J. Luo and Y. Li, *Constr. Build. Mater.*, 2021, **292**, 123434.
81 X. Ye, Y. Li, Y. Zhang and P. Wang, *J. Bionic Eng.*, 2022, **19**, 853–876.
82 M. Wang, Y. Yu, Y. Liang, Z. Han, C. Liu, S. Ma, Z. Lin and L. Ren, *J. Bionic Eng.*, 2022, **19**, 1439–1448.
83 M. Paolieri, Z. Chen, F. Babu Kadumudi, M. Alehosseini, M. Zorrón, A. Dolatshahi-Pirouz and H. Maleki, *ACS Appl. Nano Mater.*, 2023, **6**, 5211–5223.
84 N. Yang, X. Yin, H. Liu, X. Yan, X. Zhou, F. Wang, X. Zhang, Y. Zhao and T. Cheng, *ACS Appl. Mater. Interfaces*, 2023, **15**, 42992–43002.
85 Y. Xiong, Y. Zhao, Y. Tao, F. Yao, D. Li and D. Xu, *Nano Lett.*, 2020, **20**, 8576–8583.
86 L. Meng, M. Zhang, H. Deng, B. Xu, H. Wang, Y. Wang, L. Jiang and H. Liu, *CCS Chem.*, 2021, **3**, 2194–2202.
87 M. Amjadi, A. Pichitpajongkit, S. Lee, S. Ryu and I. Park, *ACS Nano*, 2014, **8**, 5154–5163.
88 C. Peng, P. Wei, X. Li, Y. Liu, Y. Cao, H. Wang, H. Yu, F. Peng, L. Zhang, B. Zhang and K. Lv, *Nano Energy*, 2018, **53**, 97–107.
89 B. C. Tee, C. Wang, R. Allen and Z. Bao, *Nat. Nanotechnol.*, 2012, **7**, 825–832.
90 F. Han, J. Li, S. Zhao, Y. Zhang, W. Huang, G. Zhang, R. Sun and C.-P. Wong, *J. Mater. Chem. C*, 2017, **5**, 10167–10175.
91 L. Zhao, P. Yang, S. Shi, X. Wang and S. Yu, *Chem. Eng. J.*, 2023, **473**, 145156.
92 T. Hu, S. Xuan, L. Ding and X. Gong, *Sens. Actuators, B*, 2020, **314**, 128095.
93 S. Zhao, L. Guo, J. Li, N. Li, G. Zhang, Y. Gao, J. Li, D. Cao, W. Wang, Y. Jin, R. Sun and C.-P. Wong, *Small*, 2017, **13**, 1700944.
94 C. E. Owens, R. J. Headrick, S. M. Williams, A. J. Fike, M. Pasquali, G. H. McKinley and A. J. Hart, *Adv. Funct. Mater.*, 2021, **31**, 2100245.
95 X. Fu, J. Li, D. Li, L. Zhao, Z. Yuan, V. Shulga, W. Han and L. Wang, *ACS Appl. Mater. Interfaces*, 2022, **14**, 12367–12374.
96 M. Sang, K. Kang, Y. Zhang, H. Zhang, K. Kim, M. Cho, J. Shin, J. H. Hong, T. Kim, S. K. Lee, W. H. Yeo, J. W. Lee, T. Lee, B. Xu and K. J. Yu, *Adv. Mater.*, 2022, **34**, e2105865.
97 G.-H. Lee, H. Kim, J. Lee, J.-Y. Bae, C. Yang, H. Kim, H. Kang, S. Q. Choi, S. Park, S.-K. Kang, J. Kang, Z. Bao, J.-W. Jeong and S. Park, *Mater. Today*, 2023, **67**, 84–94.
98 V. Rana, P. Gangwar, J. S. Meena, A. K. Ramesh, K. N. Bhat, S. Das and P. Singh, *Nanotechnology*, 2020, **31**, 385501.
99 Y. Jung, K. Jung, B. Park, J. Choi, D. Kim, J. Park, J. Ko and H. Cho, *Micro Nano Lett.*, 2019, **7**, 20.
100 J. Li, S. Zhao, X. Zeng, W. Huang, Z. Gong, G. Zhang, R. Sun and C.-P. Wong, *ACS Appl. Mater. Interfaces*, 2016, **8**, 18954–18961.
101 X. Hui, S. Sharma, M. Sharifuzzaman, M. A. Zahed, Y. D. Shin, S. K. Seonu, H. S. Song and J. Y. Park, *Small*, 2022, **18**, e2201247.
102 S. Wang, S. Xuan, W. Jiang, W. Jiang, L. Yan, Y. Mao, M. Liu and X. Gong, *J. Mater. Chem. A*, 2015, **3**, 19790–19799.
103 W. Zhao, D. Zhang, Y. Yang, C. Du and B. Zhang, *J. Mater. Chem. A*, 2021, **9**, 22082–22094.
104 L. Ding, L. Sun, Z. Wang, D. Li, Q. Zhang, X. Liu, Y. Ren and Y. Li, *Chem. Eng. J.*, 2023, **474**, 145859.
105 Y. Wang, Y. Yue, F. Cheng, Y. Cheng, B. Ge, N. Liu and Y. Gao, *ACS Nano*, 2022, **16**, 1734–1758.
106 Q. Li, X. Zhi, Y. Xia, S. Han, W. Guo, M. Li and X. Wang, *ACS Appl. Mater. Interfaces*, 2023, **15**, 19435–19446.
107 M. Zhang, W. Yang, Z. Wang, H. Liu, R. Yin, C. Liu and C. Shen, *Appl. Phys. Lett.*, 2023, **122**, 043507.
108 H.-H. Tai, B.-A. Chen, Y.-H. Liu, Y.-J. Lu and J.-C. Wang, *IEEE Sens. J.*, 2022, **22**, 6418–6425.
109 T. Yin, Y. Cheng, Y. Hou, L. Sun, Y. Ma, J. Su, Z. Zhang, N. Liu, L. Li and Y. Gao, *Small*, 2022, **18**, e2204806.
110 K. Liu, Z. Zhou, X. Yan, X. Meng, H. Tang, K. Qu, Y. Gao, Y. Li, J. Yu and L. Li, *Polymers*, 2019, **11**, 1120.
111 L. Pan, A. Chortos, G. Yu, Y. Wang, S. Isaacson, R. Allen, Y. Shi, R. Dauskardt and Z. Bao, *Nat. Commun.*, 2014, **5**, 3002.
112 X. Wang, O. Yue, X. Liu, M. Hou and M. Zheng, *Chem. Eng. J.*, 2020, **392**, 123672.
113 Y. Li, X. Zhou, B. Sarkar, N. Gagnon-Lafrenais and F. Cicoira, *Adv. Mater.*, 2022, **34**, 2108932.
114 Y. Li, X. Li, S. Zhang, L. Liu, N. Hamad, S. R. Bobbara, D. Pasini and F. Cicoira, *Adv. Funct. Mater.*, 2020, **30**, 2002853.
115 Y. Li, S. Zhang, N. Hamad, K. Kim, L. Liu, M. Lerond and F. Cicoira, *Macromol. Biosci.*, 2020, **20**, 2000146.
116 V. Panwar and G. Anoop, *Measurement*, 2021, **168**, 108406.
117 Y.-T. Tseng, Y.-C. Lin, C.-C. Shih, H.-C. Hsieh, W.-Y. Lee, Y.-C. Chiu and W.-C. Chen, *J. Mater. Chem. C*, 2020, **8**, 6013–6024.
118 X. Zhao, W. Wang, Z. Wang, J. Wang, T. Huang, J. Dong and Q. Zhang, *Chem. Eng. J.*, 2020, **395**, 125115.
119 Y. Xia, Y. Cui, P. Huang, L. Wu, S. Du, Y. Zhu, J. Lin, X. Liu and G. Zhong, *Appl. Phys. Lett.*, 2022, **120**, 203302.
120 M. Beccatelli, M. Villani, F. Gentile, L. Bruno, D. Seletti, D. M. Nikolaidou, M. Culiolo, A. Zappettini and N. Coppedè, *ACS Appl. Polym. Mater.*, 2021, **3**, 1563–1572.
121 E. S. Muckley, J. Lynch, R. Kumar, B. Sumpter and I. N. Ivanov, *Sens. Actuators, B*, 2016, **236**, 91–98.
122 Z. Tan, H. Li, Y. Huang, X. Gong, J. Qi, J. Li, X. Chen, D. Ji, W. Lv, L. Li and W. Hu, *Composites, Part A*, 2021, **143**, 106299.
123 J. J. Lee, S. Gandla, B. Lim, S. Kang, S. Kim, S. Lee and S. Kim, *NPG Asia Mater.*, 2020, **12**, 65.

124 T. Yang and J. M. Mativetsky, *ACS Appl. Mater. Interfaces*, 2019, **11**, 26339–26345.
125 M. Galliani, L. M. Ferrari, G. Bouet, D. Eglin and E. Ismailova, *APL Bioeng.*, 2023, **7**, 016101.
126 X. Meng, L. Mo, S. Han, J. Zhao, Y. Pan, F. Wang, Y. Fang and L. Li, *Adv. Mater. Interfaces*, 2023, **10**, 2201927.
127 R. Yin, S. Yang, Q. Li, S. Zhang, H. Liu, J. Han, C. Liu and C. Shen, *Sci. Bull.*, 2020, **65**, 899–908.
128 Y. Li, P. Ding, Y. Gu, S. Qian, Y. Pang, L. Wang, J. Feng, B. Liu, Q. Wan, P. Li and Z. Liu, *Nano Res.*, 2024, **17**, 3302–3323.
129 C. Guo, A. Zhu, X. Wang, J. Dai, L. Luo, Y. Xu, B. Zeng, G. Chen and L. Dai, *Sens. Actuators, B*, 2022, **362**, 131796.
130 M. Wu, M. Pan, C. Qiao, Y. Ma, B. Yan, W. Yang, Q. Peng, L. Han and H. Zeng, *Chem. Eng. J.*, 2022, **450**, 138212.
131 Y. Zhao, N. Yang, X. Chu, F. Sun, M. U. Ali, Y. Zhang, B. Yang, Y. Cai, M. Liu, N. Gasparini, J. Zheng, C. Zhang, C. Guo and H. Meng, *Adv. Mater.*, 2023, **35**, e2211617.
132 B. Ying, R. Z. Chen, R. Zuo, J. Li and X. Liu, *Adv. Funct. Mater.*, 2021, **31**, 2104665.
133 Y. Yuan and N. Solin, *ACS Appl. Bio Mater.*, 2022, **5**, 3360–3370.
134 S. Dai, S. Wang, X. Dong, X. Xu, X. Cao, Y. Chen, X. Zhou, J. Ding and N. Yuan, *J. Mater. Chem. C*, 2019, **7**, 14581–14587.
135 R. Fu, L. Tu, Y. Zhou, L. Fan, F. Zhang, Z. Wang, J. Xing, D. Chen, C. Deng, G. Tan, P. Yu, L. Zhou and C. Ning, *Chem. Mater.*, 2019, **31**, 9850–9860.
136 J. Wang, X. Yue, X. Li, J. Dong, Q. Zhang and X. Zhao, *ACS Appl. Polym. Mater.*, 2022, **4**, 3205–3216.
137 L. Chen, Z. G. Yu, D. Liang, S. Li, W. C. Tan, Y.-W. Zhang and K.-W. Ang, *Nano Energy*, 2020, **76**, 105020.
138 X. Pang, Q. Zhang, Y. Shao, M. Liu, D. Zhang and Y. Zhao, *Sensors*, 2021, **21**, 1130.
139 Z. Kang, X. Li, X. Zhao, X. Wang, J. Shen, H. Wei and X. Zhu, *Nanomaterials*, 2023, **13**, 4.
140 Y.-F. Fu, Y.-Q. Li, Y.-F. Liu, P. Huang, N. Hu and S.-Y. Fu, *ACS Appl. Mater. Interfaces*, 2018, **10**, 35503–35509.
141 H. S. Jo, C.-W. Park, S. An, A. Aldalbahi, M. El-Newehy, S. S. Park, A. L. Yarin and S. S. Yoon, *NPG Asia Mater.*, 2022, **14**, 23.
142 M. Zhang, W. Yang, Z. Wang, H. Liu, R. Yin, C. Liu and C. Shen, *Appl. Phys. Lett.*, 2023, **122**, 043507.
143 Y. Yuan and N. Solin, *ACS Appl. Bio Mater.*, 2022, **5**, 3360–3370.
144 H.-H. Jang, J.-S. Park and B. Choi, *Sens. Actuators, A*, 2019, **286**, 107–114.
145 F. Yuan, S. Wang, S. Zhang, Y. Wang, S. Xuan and X. Gong, *J. Mater. Chem. C*, 2019, **7**, 8412–8422.
146 S. R. A. Ruth, V. R. Feig, H. Tran and Z. Bao, *Adv. Funct. Mater.*, 2020, **30**, 2003491.
147 D. Du, X. Ma, W. An and S. Yu, *Measurement*, 2022, **201**, 111645.
148 Y. Wang, W. Zhu, Y. Deng, P. Zhu, Y. Yu, S. Hu and R. Zhang, *J. Mater. Sci. Technol.*, 2022, **103**, 1–7.
149 S. Song, C. Zhang, W. Li, J. Wang, P. Rao, J. Wang, T. Li and Y. Zhang, *Nano Energy*, 2022, **100**, 107513.
150 Y. Wang, S. Dai, D. Mei and J. Jin, *IEEE Trans. Instrum. Meas.*, 2022, **71**, 1–10.
151 S. Chun, D. W. Kim, S. Baik, H. J. Lee, J. H. Lee, S. H. Bhang and C. Pang, *Adv. Funct. Mater.*, 2018, **28**, 1805224.
152 N. Bai, L. Wang, Y. Xue, Y. Wang, X. Hou, G. Li, Y. Zhang, M. Cai, L. Zhao, F. Guan, X. Wei and C. F. Guo, *ACS Nano*, 2022, **16**, 4338–4347.
153 J. Kim, M. Lee, H. J. Shim, R. Ghaffari, H. R. Cho, D. Son, Y. H. Jung, M. Soh, C. Choi, S. Jung, K. Chu, D. Jeon, S.-T. Lee, J. H. Kim, S. H. Choi, T. Hyeon and D.-H. Kim, *Nat. Commun.*, 2014, **5**, 5747.
154 Y. Xiang, L. Fang, F. Wu, S. Zhang, H. Ruan, H. Luo, H. Zhang, W. Li, X. Long, B. Hu and M. Zhou, *Adv. Mater. Technol.*, 2021, **6**, 2001157.
155 S. Chun, W. Son, C. Choi, H. Min, J. Kim, H. J. Lee, D. Kim, C. Kim, J. S. Koh and C. Pang, *ACS Appl. Mater. Interfaces*, 2019, **11**, 13608–13615.
156 Y. Lu, Y. He, J. Qiao, X. Niu, X. Li, H. Liu and L. Liu, *ACS Appl. Mater. Interfaces*, 2020, **12**, 55169–55180.
157 L. Ding, S. Xuan, L. Pei, S. Wang, T. Hu, S. Zhang and X. Gong, *ACS Appl. Mater. Interfaces*, 2018, **10**, 30774–30784.
158 X.-D. Li and H.-X. Huang, *Polym. Eng. Sci.*, 2023, **63**, 1678–1690.
159 C. Pang, G.-Y. Lee, T.-I. Kim, S. M. Kim, H. N. Kim, S.-H. Ahn and K.-Y. Suh, *Nat. Mater.*, 2012, **11**, 795–801.
160 L. Ding, L. Pei, S. Xuan, X. Fan, X. Cao, Y. Wang and X. Gong, *Adv. Electron. Mater.*, 2020, **6**, 1900653.
161 S. Zhao and R. Zhu, *Adv. Mater. Technol.*, 2019, **4**, 1900414.
162 F. Lin and W. Cheng, *Adv. Electron. Mater.*, 2023, **9**, 2300334.
163 X. Fu, Z. Zhuang, Y. Zhao, B. Liu, Y. Liao, Z. Yu, P. Yang and K. Liu, *ACS Appl. Mater. Interfaces*, 2022, **14**, 44792–44798.
164 E. Karner-Petritz, A. Petritz, T. Uemura, N. Namba, T. Araki, T. Sekitani and B. Stadlober, *Adv. Electron. Mater.*, 2023, **9**, 2201333.
165 J. Zhao, J. Luo, Z. Zhou, C. Zheng, J. Gui, J. Gao and R. Xu, *Sens. Actuators, A*, 2021, **323**, 112658.
166 X.-F. Zhao, C.-Z. Hang, X.-H. Wen, M.-Y. Liu, H. Zhang, F. Yang, R.-G. Ma, J.-C. Wang, D. W. Zhang and H.-L. Lu, *ACS Appl. Mater. Interfaces*, 2020, **12**, 14136–14144.
167 Z. Qiu, J. Martínez-Sánchez, P. Arias-Sánchez and R. Rashdi, *Inf. Fusion*, 2023, **97**, 101806.
168 Y. Song, F. Wang and Z. Zhang, *Micromachines*, 2018, **9**, 236.
169 T. Yuan, R. Yin, C. Li, C. Wang, Z. Fan and L. Pan, *Chem. Eng. J.*, 2023, **473**, 145475.
170 W. Zhang, H. Ma and S. X. Yang, *Expert Syst. Appl.*, 2015, **42**, 1039–1049.
171 Z. Wang, Z. Qin, B. Zhao, H. Zhu and K. Pan, *J. Mater. Chem. C*, 2023, **11**, 14641–14651.
172 C. Huang, Y. Wang, Y. Cheng, Z. Qi, A. Liu, Q. Deng and N. Hu, *Compos. Sci. Technol.*, 2022, **226**, 109549.
173 A. Kaidarova, N. Alsharif, B. N. M. Oliveira, M. Marengo, N. R. Geraldi, C. M. Duarte and J. Kosel, *Glob. Chall.*, 2020, **4**, 2000001.
174 G. Tian, K. Xu, Y. Huang, X. You, W. Yu, H. Liu, J. Li, J. Liu, X. Jin, H. Li, Q. Ke and C. Huang, *J. Mater. Chem. A*, 2023, **11**, 21333–21344.

175 C. Zhao, F. M. Li, X. Y. Pan, S. Li, Y. F. Zhai, S. Fahad, H. Y. Yu and M. Wang, *IEEE Sens. J.*, 2023, **23**, 12607–12617.
176 Y. Li, M. Zhao, Y. Yan, L. He, Y. Wang, Z. Xiong, S. Wang, Y. Bai, F. Sun, Q. Lu, Y. Wang, T. Li and T. Zhang, *npj Flexible Electron.*, 2022, **6**, 46.
177 P. Xiao, W. Zhou, Y. Liang, S.-W. Kuo, Q. Yang and T. Chen, *Adv. Funct. Mater.*, 2022, **32**, 2201812.
178 J. Qu, B. Mao, Z. Li, Y. Xu, K. Zhou, X. Cao, Q. Fan, M. Xu, B. Liang, H. Liu, X. Wang and X. Wang, *Adv. Funct. Mater.*, 2023, **33**, 2306249.
179 H. Wang, H. Yang, S. Zhang, L. Zhang, J. Li and X. Zeng, *Adv. Mater. Technol.*, 2019, **4**, 1900147.
180 M. Amit, L. Chukoskie, A. J. Skalsky, H. Garudadri and T. N. Ng, *Adv. Funct. Mater.*, 2020, **30**, 1905241.
181 Y. Park, K. Kwon, S. S. Kwak, D. S. Yang, J. W. Kwak, H. Luan, T. S. Chung, K. S. Chun, J. U. Kim, H. Jang, H. Ryu, H. Jeong, S. M. Won, Y. J. Kang, M. Zhang, D. Pontes, B. R. Kampmeier, S. H. Seo, J. Zhao, I. Jung, Y. Huang, S. Xu and J. A. Rogers, *Sci. Adv.*, 2020, **6**, eabe1655.
182 H. Zhang, R. He, H. Liu, Y. Niu, Z. Li, F. Han, J. Li, X. Zhang and F. Xu, *Sens. Actuators, A*, 2021, **322**, 112611.
183 Z. Zhang, Z. Chen, Y. Wang and Y. Zhao, *Proc. Natl. Acad. Sci. U.S.A.*, 2020, **117**, 18310–18316.
184 C. Zhang, S. Liu, X. Huang, W. Guo, Y. Li and H. Wu, *Nano Energy*, 2019, **62**, 164–170.
185 C. Zhong, S. Zhao, Y. Liu, Z. Li, Z. Kan and Y. Feng, *Robotica*, 2022, **41**, 1025–1038.
186 Z. Zou, C. Zhu, Y. Li, X. Lei, W. Zhang and J. Xiao, *Sci. Adv.*, 2018, **4**, eaaq0508.
187 H. S. Jo, S. An, C.-W. Park, D.-Y. Woo, A. L. Yarin and S. S. Yoon, *ACS Appl. Mater. Interfaces*, 2019, **11**, 40232–40242.